Computational Modelling Of Plant Root Architecture and Fluid Absorption through Filtration Media Populated By Root Structures

For Group Project:

Investigating Stormwater Filters and Bioretention Systems

A Study on the *Hydro Filterra*(TM) System Manufactured by *Hydro-International* (UK)

Individual Report – I2

JAMES RONALD
015341
580007258
2012

Supervisor: Dr Gavin Tabor

INDEX

1.0 Introduction 1

1.1 Aims and Objectives 5

1.2 Group Roles 5

2.0 Micro-Scale Modelling of Root Branch Structures 6

2.1 Hydraulic Conductivity of Root Branches 6

2.2 Computed Tomography Scanning 7

2.3 Preliminary Assessment of CT Scan Capabilities 8

2.4 Root Branch Model 10

3.0 Macro Scale Modelling of Plant Root Architecture 13

3.1 Soil-Water Uptake by Plant Root Architecture 13

3.2 Root Architecture Modelling 14

3.3 Macro-Scale Computational Modelling 16

4.0 Results and Discussion 19

4.1 Results of the Micro Scale Investigation 19

4.1.1 Radial Conductivity 19

4.1.2 Axial Conductivity 23

4.1.3 Visual analysis 25

4.2 Results of the Macro Scale Investigation 28

4.2.1 Mesh Refinement 28

4.2.2 Effects of Root Architecture upon soil Hydraulic Conductivity 29

5.0 The *Hydro Filterra*^{TM} Model 34

5.2 Establishing a Representation of the *Hydro Filterra*^{TM} System 34

5.3 Results of the *Hydro Filterra*^{TM} Simulation 35

6.0 Conclusions 36

7.0 References 39

8.0 Appendix 42

8.1 The Van Genuchten Model 42

8.2 Penman Monteith Equation 42

8.3 Penman Monteith Variables 44

8.4 Micro-Scale Investigation Data 44

8.5 Macro Scale Investigation Data 46

Abstract

The absorption characteristics of root structures are considered computationally on the micro and the macro scales. The radial conductivity of individual branches are assessed through the incorporation of micro CT techniques, wherein the radial absorption parameter is shown to increase with extended structure radius. An assessment of the changes in fluid velocity and total driving pressure across the boundary highlight the impacts of soil structure upon the flow regime and yield a description of flow around two competing branch structures. A macro scale root architecture model is presented within a homogenous porous region representative of the *Hydro Filterra* soil composition and a global absorption characteristic, based on the transpiration rate of the biological system, defines the redirection of flow into the root topology. The consequential effects of root architecture upon the hydraulic conductivity of the porous medium are seen to include that of an increased magnitude of hydraulic conductivity in the immediate area of the branch structures, where the effects are negated given a set distance from the root tip.

Keywords: *radial absorption, micro CT, soil composition, root architecture, hydraulic conductivity*

List of Figures

Figure 1 The *Hydro Filterra*™ bioretention system comprising of four key features.

Figure 2 Flow chart presenting the inter-relation of work to be carried out by the group

Figure 3 Simplified illustration of the CT scan process

Figure 4 Segmented root structures, obtained via CT scan techniques

Figure 5 a) Surface topology of *sample C* without surface smoothing filter applied

b) Surface topology of *sample C* with smoothing filter applied

Figure 6 First order root branch extracted from *Malus Evereste* with *Region A* section

Figure 7 Composition of *Region A* established through CT results.

Figure 8 Cross-section regions highlighting the quality of the discretised mesh

Figure 9 Computational model of a plant root system

Figure 10 Data contained within the case file *porousZones*

Figure 11 Schematic of the control volume with incorporated porous regions

Figure 12 Computational mesh of the root architecture model

Figure 13 Illustration of the position of the data lines close to the *Central Offshoot* branch

Figure 14 Comparison of the changes in total fluid pressure with flow velocity across the boundary of the *Central Offshoot* branch

Figure 15 Comparison of the changes in total fluid pressure with flow velocity across the boundary of the *Side Offshoot* branch

Figure 16 Comparison of the changes in total fluid pressure with flow velocity across the boundary of the *Main Stem* branch

Figure 17 Additional comparisons of the changes in total fluid pressure with flow velocity across the boundary of the *Main Stem* branch

Figure 18 Graphical representation of the change in root hydraulic conductivity with increased root diameter

Figure 19 Comparison of the axial conductivity of the *Main Stem*, *Central Offshoot* and *Side Offshoot* branches to that of experimental data

Figure 20 Velocity contour plot of fluid moving through the root soil region *Plane 1*

Figure 21 Velocity contour plot of fluid moving through the root soil region *Plane 2*

Figure 22 Velocity contour plot of fluid moving through the root soil region *Plane 3*

Figure 23 Three dimensional representation of the root soil zone with roots

Figure 24 Graphical representation of the convergence of the mesh towards geometrical accuracy

Figure 25 Comparison of the hydraulic conductivity of a porous region not occupied by root structures to that of a region which incorporates root architecture.

Figure 26 Comparison of the changes in total pressure with distance from the main stem for increasing velocities

Figure 27 Pressure contour plot of a porous region not occupied by root architecture

Figure 28 Pressure contour plot of a porous region surrounding a root system

Figure 29 Description of the changes in the hydraulic conductivity of soil with distance from the main stem

Figure 30 Schematic presenting the positions of sample data lines

Figure 31 Comparative changes in hydraulic conductivity along sample lines *C* and *D*

Figure 32 Computational representation of the Hydro Filterra™ bioretention system and the surrounding road surface

Figure 33 Computational mesh of the case geometry

Figure 34 Three dimensional representation of the case geometry at time step t=0

Figure 35 Table of values containing the parameters presented in equations (8.0) to (8.11)

Figure 36 Total Pressure contour plot for the data slice *Plane 2*

Figure 37 Total Pressure contour plot for the data slice *Plane 1*

Figure 38 Total Pressure contour plot for the data slice *Plane 3*

Figure 39 Table of values containing the parameters of the mesh refinement process

1.0 Introduction

Increased urbanisation within the past decade has prompted developments in stormwater management systems and the improvement of rainwater harvesting techniques that seek to actively control levels of surface runoff. The necessity for pollutant removal from urban water systems is highlighted by the increased legislative demands being set by the EU, such as that of the Water Framework Directive (WFD), which seeks to launch an improved environmental awareness of the implications of stormwater runoff. The overall effects of increased surface runoff can range from the destruction of ecological systems, via the transference of chemicals into rivers, to the detrimental effects brought about by flooding. Currently, control systems have consisted of transporting wastewater to processing plants, where large amounts of energy is consumed during the formulation of biosolids. This report, however, examines the potential of a small scale bioretention system that can be used to remove pollutants from surface runoff, thus potentially reducing the total energy consumption of processing plants and minimising the effects of water pollution.

Hydro International (UK), a leader in the development of technology aimed at controlling urban water runoff, specialises in the construction of bioretention systems, such as that of the *Hydro Filterra*^{TM} design, capable of remove 85% of pollutants from within stormwater runoff (*Hydro Filterra*^{TM} TM Design Guide). The *Hydro Filterra*^{TM} system, presented in Figure 1, incorporates a specialised soil medium to immobilise and retain large and small scale contaminants that are being transported through the structure. This region is located between a dissipative mulch layer and a gravel base layer. The structure also utilises a biological plant system to absorb micro-scale contaminants, such as Nitrogen and Phosphorus, and retain any heavy metals being carried within the fluid. Thus, the combination of an engineered filtration media and a biological plant system allows for the establishment of an efficient design, capable of being implemented into a variety of locations.

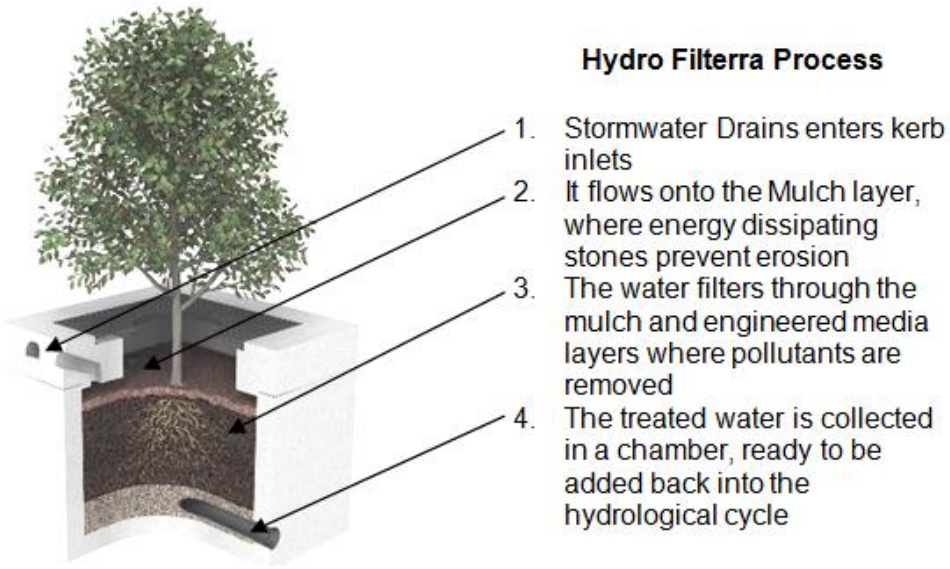

Figure 1 – The Hydro Filterra^{TM} *bioretention system comprising of four key features.*
(Hydro Filterra^{TM} *– Advanced Bioretention System for Stormwater Treatment: Design Guide)*

The role of root architecture within the filtration medium serves to maintain the structure of the surrounding soil and ensure a sufficient level of fluid absorption necessary to sustain the biological system. The presence of a root structure allows for the immobilisation of surrounding heavy metals, dissolved within the flow regime, and the breakdown of contaminants such as nitrogen and phosphorus. Additionally, the continuous expansion and contraction of the root system during periods of irregular rainfall can lead to the development of preferential flow pathways, thus decreasing the level of soil resistance and elevating infiltration rates. The importance of the biological system is highlighted by the formation of pockets of aerobic and anaerobic conditions, which allow microbial systems to thrive. Microorganisms within the soil can lead to variations in soil pH and can enhance biological processes such as nitrification and denitrification for regions with aerobic and anaerobic properties respectively. The immobilisation of dissolved metals has also been shown to be possible within such conditions through experimental studies carried out by Clark and Pitt (2009). However, some processes, such as the breakdown of nitrate and phosphorus, have been identified to rely solely upon the less prevalent anaerobic environment. Overall, the *Hydro Filterra*^{TM} bioretention system relies upon both a filtration media and a biological system to immobilise and remove a number of key contaminants from stormwater surface flow.

An important aspect to consider when assessing the role of root architecture within a filtration media is that of the relationship between soil structure and plant root growth patterns. Soil structure is essential to the functioning of water, nutrient and gas fluxes through the region and is responsible for the growth of organic matter. Work undertaken by Angers and Caron (1998) assesses the role of plant roots in modifying the strength of this structure and examines the effects of root growth mechanisms upon soil compaction. The studies suggests that soil stability, defined by its resistance to applied stresses, is primarily affected by the process of wetting and drying, leading to the formation of cracks within the soil clusters. These clusters can subsequently become separated due to the stresses induced by root growth. The study goes on to suggest that there exists a positive relationship between soil particle compaction and the overall soil strength. Thus, the overall soil strength is enhanced by hydraulic suction, which aids in the compaction of soils. This is verified by work from Horn et al. (1994), which examines the effects of soil saturation upon particle cluster strength through the use of experimental methodology.

The growth patterns of root structures in response to given soil characteristics have also been extensively researched within the biological community with key findings being presented within a study by Sachs and Molisch (1983), wherein plant root structures are shown to respond positively to a hydraulic stimulus. The work offers findings that a number of root branches will change their direction of development in accordance with previously established pockets of moisture, thus demonstrating that root growth patterns are not only dependent upon soil structure, but the availability of moisture as well. This work was validated by Hooker (1986) wherein roots were presented to mature according to moisture availability when grown in a water vapour gradient without the impedance of a soil system.

The development of root systems is considered to be largely a complex subject, where numerous studies have been in based around that of investigating the internal structure of the root branch. In general, root systems have been revealed to incorporate a number of adaptations that allow them to perform their primary functions of anchorage, absorption and nutrient storage. In order to accurately simulate these processes, it is necessary to first understand the biological processes associated with their function. Advances in transmission electron microscopy (TEM) have revealed details regarding the internal structure of plant root systems and can be seen to include studies such as those carried out by McCulley et al. (1993), within which the structure of the permeable epidermis is revealed to consist of a number of layers that mature during root branch growth. The maturation of these surfaces increases shoot strength, allowing for more successful penetration and a greater overall resistance to

deformation. More importantly, however is the method of absorption shown through the use of TEM for a maize root tip, as presented within the same study. Findings show an epidermal thickness of 6μm through which the fluid must pass before being transported up the plant. Since this region is shown to contain a number of cells that restrict the movement of fluid, it is proposed that the time taken to reach the centre of the root will vary for different density root systems, thus resulting in contrasting absorption rates for fibrous and dense root systems.

The derivation of mathematical notation and computational methodology describing soil water uptake by these plant root systems can be seen to be primarily hindered by the complexity of the biological system. In addition to the anisotropic nature of the root-soil interface, variations in plant root cell size and the unpredictability of root growth patterns all present a number of challenges to overcome in order to accurately depict a root system. The large number of dependencies between plant root growth and soil structure mean that the benefits of experimental analysis outweigh the practicality of predicting root growth mathematically or computationally. Nevertheless, due to the relationships between biological, climatic and hydrological systems, one can isolate a number of features required in order to accurately depict a plant root system and thus derive a model capable of analysing micro-scale contaminant removal.

The most important aspect to include within a plant root architecture model is that of the description of the total fluid uptake by plant root systems. When considering absorption models, one can distinguish between two main approaches. The first considers the root structure on a micro-scale, in which soil water uptake is represented as a radial flux across a single root interface, driven by a water potential gradient. Root architecture is then built up as a series of connecting axis at specific orientations. The second method considers the structure on a macro-scale, regarding the root system as an abstract object with consistent absorption properties. A sink term, based upon an energy consumption parameter, is then applied to the continuity equation for soil water transport.

A literary analysis of micro-scale models relating to the biological networking of systems revealed developments in methodology regarding the parameterisation of radial water and energy flux across permeable root interfaces (Feddes and Raats, 2004). The study examines the level of detail required to accurately parameterise a regional scale plant root network through the use of micro-scale methodology. The approach incorporates a water potential gradient between the root and soil regions to describe fluid flow across the root boundary. The study gives a realistic representation of temporal changes in water content and provides methodology applicable to root architecture modelling, but is limited by the amount of data required relating to root architecture geometry and soil heterogeneity. In addition, the model generalises the topology of the structure and thus neglects the effects of soil depth and soil particle compaction.

Alternative methodology for plant root architecture modelling is explored within work carried out by Simunek and Hopmans (2008) and Feddes et al. (1976) wherein plant root architecture is modelled on the macro-scale. The latter study explores the relationship between changes in soil water content and root water uptake rate, thus establishing accurate notation describing the temporal change in volumetric water content for soil surrounding a generic root structure. Work undertaken by Simunek and Hopmans (2008) advances on this, presenting a threshold value above which reductions in root water uptake in soil water stressed regions are compensated by increased in root water uptake rates in non-stressed regions. The principal methodology used within both studies integrates the use of a partial differential equation to model changes in volumetric water content over time, incorporating a soil hydraulic conductivity parameter and a sink term to represent the percentage volume of water removed from a unit volume of soil at a given saturation. The sink term is modelled proportionally to the potential transpiration rate, which is established through the assessment of the atmospheric demand, and is distributed over the entire root zone according to root length density. The

progression of this work, as carried out by Simunek and Hopmans (2008), implicates a critical water stress index in which, if not reached, results in a much larger pressure gradient across the root boundary for regions of non-stressed soil water content. Both studies can be seen to give a comprehensive representation of soil water movement into the root zone via the incorporation of a sink term and the utilisation of a pressure differential across the boundary. However, the notation neglects any radial variation and assumes a constant conductivity for the root biomass. Work carried out by Neumann (2002) suggests that root absorption rate is heavily dependent upon root density and root depth. Thus, by generalising the total root water uptake into a single sink term, the overall accuracy of the model is reduced.

A final method for modelling root soil interactions can be seen to be highlighted by work within work by Hector et al. (1992), which presents methodology for illustrating changes in the hydraulic conductivity of soil with distance from the root structure. The report examines water extraction by crop root systems, whereby the entire soil root system is modelled as a resistance network diagram, based upon a layered soil regime. Spatial changes in soil water content are represented as a function of root density, soil water potential and a parameter defining the medium's total resistance to water uptake per unit length of root branch. The model applies layer dependant resistivity factors to the entire root zone, which encompass the root's radial resistance, axial resistance and interface resistance. Each layer is also modelled with a specific hydraulic potential and a variable depth. Thus the total inflow of fluid into the root zone is spatially modelled through the application of Kirchhoff's voltage laws, whereby the driving force is represented as the hydraulic potential and the resistance is represented as the root's resistance to flow. This method can be seen to have significant benefits when developing a computational root architecture model in three dimensions, as it simplifies the relative rates of uptake for varying soil depths. In addition, it incorporates a root density parameter and integrates a radial resistance to fluid absorption. However, the model is somewhat limited in that it utilises a number of empirical values, such as the radial and axial resistances to fluid inflow, and bares no relation to atmospheric conditions or rainfall patterns. Furthermore, the model has limited flexibility and may be inapplicable to a root zone with extensive root branching. Thus, a less complex computational investigation of the hydraulic conductivity of plant root architecture was pursued in order to better understand the effects of root structures upon the removal of fluid from the *Hydro Filterra*^{TM} bioretention system.

In this paper, the uptake of fluid by a root system is thoroughly investigated through the utilisation of both micro-scale and macro-scale computational techniques. The impacts of soil structure upon preferential flow pathways are explored through the incorporation of computed tomography scanning techniques and the effects of root geometry are analysed on a micro-scale with respect to the radial conductivity of root structures. The macro-scale effects of root architecture upon the porosity of the surrounding medium are considered through the application of global absorption parameter to a macro-scale computational model and the impacts of soil water absorption upon the outlet flow conditions are explored through the implementation of the macro-scale model into that of a collaborative model, which describes the *Hydro Filterra*^{TM} bioretention system as whole. The theoretical components of fluid absorption are presented in §2 and the rest of the paper is organised as follows: The basic concepts and applicability of computed tomography scanning are discussed and applied to a suitable biological structure in §2. Details of the global absorption characteristic are presented in §3, as well as the specifics regarding the construction of a full macro-scale model. In §4, the results of the micro-scale and macro-scale computational simulations are discussed, followed by a discussion of the collaborative model in §5. Concluding remarks are presented §6.

1.1 Aims and Objectives

The *Hydro Filterra*^{TM} bioretention system utilises a plant system to aid in the removal of contaminants, such as phosphorus and nitrogen. It is therefore of importance that the roles of the root system are fully investigated. The key aims of the study will be to accurately simulate the uptake of fluid by root architecture, whilst also integrating an accurate representation of the porosity of the surrounding soil. In addition, the effects of root branch geometry upon the conductivity of the system should be assessed with respect to the composition of the surrounding soil. Finally, the results of should be comparable to that of empirical data, thus validating the computational methodology.

The key objectives of the report are as follows:

1. Develop a stable and accurate three dimensional computational model for the flow around plant root architecture in a porous region, using the values obtained from a micro-scale analysis of the soil, which is to be carried out by A. Begley.
2. Computationally determine the characteristics of fluid flow through a soil region that contains root structures and assess the implications of root topology upon total absorption.
3. Use empirical values for root water uptake by plant systems to validate the computational results.

1.2 Group Roles

Specific aspects of the bioretention system are to be investigated both experimentally and computationally by individual members of the group, thus bringing about a collaborative assessment of the entire bioretention system. Figure 2 presents a flow diagram that associates the work carried out by the experimental team to that of the computational work undertaken by the CFD team. In addition to the work carried out regarding the soil region, an assessment of the properties of the container and an investigation of the characteristics of the inlet vents will allow for a description of the importance of the external features. Thus, when compiled with work regarding the layout of the surrounding area and the positioning of the bioretention units, an overview of the effectiveness of the *Hydro Filterra*^{TM} units can be established and a computational representation of the nature of flow through the entire system can be derived.

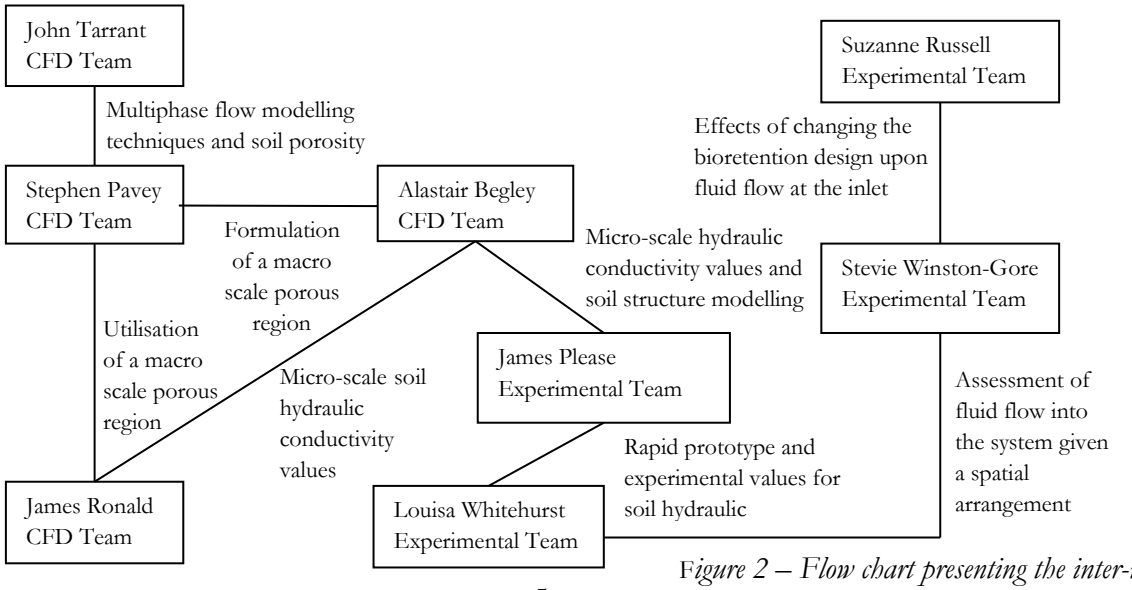

Figure 2 – Flow chart presenting the inter-relation of work to be carried out by the group

2.0 Micro-Scale Modelling of Root Branch Structures

2.1 Hydraulic Conductivity of Root Branches

The analysis of soil-water uptake by a single root system can be considered on a micro-scale basis. Primarily, micro-scale modelling techniques work to assess the implications of soil compaction upon root water uptake and to demonstrate the key differences in radial conductivity for roots of differing radii. The major benefits of micro-scale modelling can be seen to include that of taking into account the true effects of surface topology upon the radial conductivity and allowing for the consideration of soil particle conductivity, which may bring about temporal changes in soil water content. In this section, the methodology for analysing the hydraulic conductivity of single root structures is presented, thus allowing for an analysis of the effects of root geometry upon the total absorption level.

The hydraulic conductivity parameter is a property of the root structure that describes the ease with which fluid can move into the system. It is dependent upon the permeability of the circumferential surface and the total soil saturation in the immediate vicinity of the root and can be seen to be inversely proportional to root's resistive properties. The hydraulic conductivity is established by considering the fluid flux in the axial and radial directions, where the radial flux is primarily dependent upon a radial pressure gradient and the axial flux is driven by the evaporation of fluid higher up the plant.

The characteristic axial movement of fluid through the xylem vessels of the plant is described through the implementation of the Hagen-Poisueille equation (2.1), which considers the axial flux of a laminar incompressible fluid through a cylindrical pipe system:

$$q_z = -k_z \left(\frac{dp_r}{dz} - \rho g\right) \qquad (2.1)$$

Where q_z [$m^3 s^{-1}$] is the axial flux, p_r [Pa] is the internal root pressure of the xylem vessels, and z[m] is position along the root with respect to the base to the stem. The root axial conductivity parameter, k_z [$m^4 s^{-1} Pa^{-1}$], is the summation of the fluxes through xylem vessels with differing radii and is defined as:

$$k_z = \Sigma \frac{\pi n_i {R_i}^4}{8\mu} \qquad (2.2)$$

Where R_i [m] is the radius of the xylem vessel, n_i is the number of xylem vessels with radius R_i per cross sectional area of the root, the subscript i is an index for different radius categories and μ[Pa s^{-1}] is the dynamic viscosity of water.

The radial component of flux is derived through an assessment of the pressure difference between the internal and external regions and is dependent upon a radial conductivity factor, k_r, which defines the root's resistance to radial flow:

$$q_r = k_r A_r (p - p_r) \qquad (2.3)$$

Where q_r [$m^3 s^{-1}$] represents the radial flux, k_r [m Pa^{-1} s^{-1}] is the radial conductivity, p [Pa] is the pore pressure in the soil and A_r [m^2] is the surface area of the root structure. Crucially, the variable *p* is a function of the soil saturation, which can be derived through the utilisation of a

water retention curve or the Van Genuchten mathematical approach (Van Genuchten 1980). Essentially, the Van Genuchten approach can be seen to be a mathematical representation of the water retention curve, which incorporates several empirical values. The details of this approach can be found within Section 8.1 of the Appendix.

The key limiting cases for this model have been shown to include that of cases where the resistance to radial flow is small in comparison to the resistance to axial flow and cases where the internal fluid pressure is roughly equal to the external soil pore pressure, thus limiting the total radial driving force (A. C. Fowler et al. 2004). The first case can be seen to be primarily applicable to thin roots and extremely low order branches, wherein a thin cortex layer brings about a high radial conductivity. However, the axial conductivity can be seen to be greatly affected by decreases in root diameter, since the axial flux scales with the fourth power of the xylem radius and the total number of vessels, as presented within equation (2.2). Thus, the total level of fluid uptake becomes negligible for small, thin roots. The latter case refers to the radial absorption of higher order roots of increased diameter, wherein the key resistance to the absorption of fluid is brought about due to an increased cortex thickness. Thus, for situations where high soil water content can be identified within the vicinity of a thick root structure, the total level of absorption is primarily limited by the high radial resistance of the system (T. Roose et al. 2011).

2.2 Computed Tomography Scanning

Root systems play an integral part in soil-based resource acquisition, but can be difficult to model both mathematically and computationally due to their structural complexity. In order to accurately establish a root topology model that takes the adjacent soil structure into consideration, one can implement high resolution computed tomography (CT) scanning techniques to define a three dimensional visualisation of the root system in situ. Thus, the effects of soil porosity and plant soil interaction can be modelled with a high level of precision in a non-destructive manner.

Micro CT scanning is a common method of data collection wherein a three dimensional representation of a system is built up through the collation of a number of X-ray images, taken at varying orientations. Typically, the series of X-ray data slices are generated using an X-ray source that rotates about an object, as presented within Figure 3. As the X-ray emitter rotates about the object, specific levels of X-ray attenuation bring about differences in grey scale level within each CT slice. The total degree of X-ray attenuation is dependent upon the density of matter and thus can be used to formulate a representation of the object composition.

The main advantages of using micro CT methods to derive a computational model can be seen to include that of the ability to produce a high resolution image and the capability to measure extremely small areas of interest to a high degree of detail. In contrast to CT scan techniques, the alternative MRI scan method can be seen to produce images that incorporate a lower level of detail and have been shown to respond poorly to external interference such as that of vibrations in the surrounding area or the inclusion of dust particles within the sample. Regardless of the disadvantages of the MRI technique, the CT scan approach was adopted due to the availability of resources and a limited cost incursion.

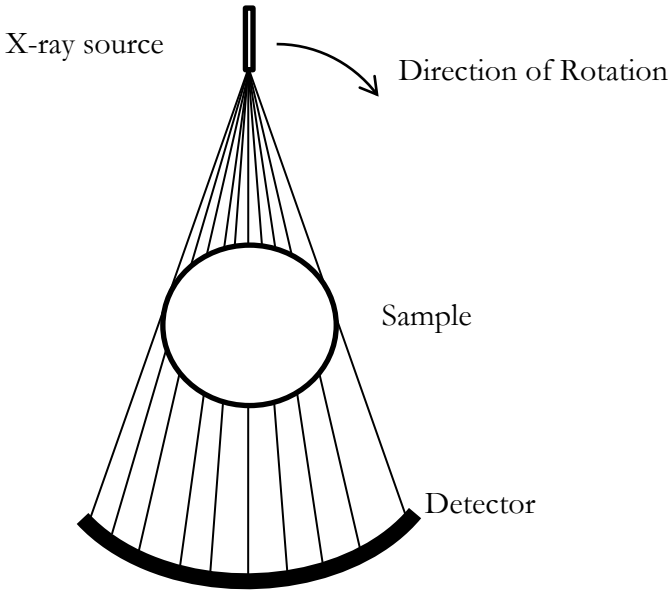

Figure 3 – Simplified illustration of the CT scan process

2.3 Preliminary Assessment of CT Scan Capabilities

The process of utilising micro CT scanning to examine biological systems such as that of root architecture has been shown to be somewhat problematic for specific cases that involve the analysis of numerous similar density artefacts (R. Lontoc et al. 2006) (J Nemirovski 2006). When scanning systems such as this, the researcher can encounter two fundamental problems; beam hardening and low contrast resolution. Beam hardening can be seen to be the phenomena wherein the edges of the image appear brighter than that of the internal region and can be seen to be brought about by changes in x-ray energy when moving through the medium, thus causing a higher degree of attenuation near the centre of the object. This leads to problems when trying to segment specific regions of the scan. Low resolution imaging can be seen to be directly related to the presence of multiple similar density articles within a small region which has been shown to be amplified for small scale samples.

In order to assess the capabilities of the available equipment, a preliminary study was undertaken to determine the key problematic areas that could be encountered. The study entailed the removal of five root systems from living plant organisms, wherein two of the samples (samples 4b and 4c) can be seen to be extracted from the same organism, but differ in terms of root order. The samples presented in Figure 4 were extracted with the aim of preserving the structure of the surrounding soil and with the intention of ensuring that all root branches remained attached.

The root systems were incorporated into a 1mm thick glass test tube which was 25mm in diameter and 75mm high. The choice of container was to ensure that the medium surrounding the sample was if dissimilar density to that of the soil and of the root structures. Finally, a key point to note is that of the resolution of the image, where the resolution of all the presented samples can be identified as 26.7microns.

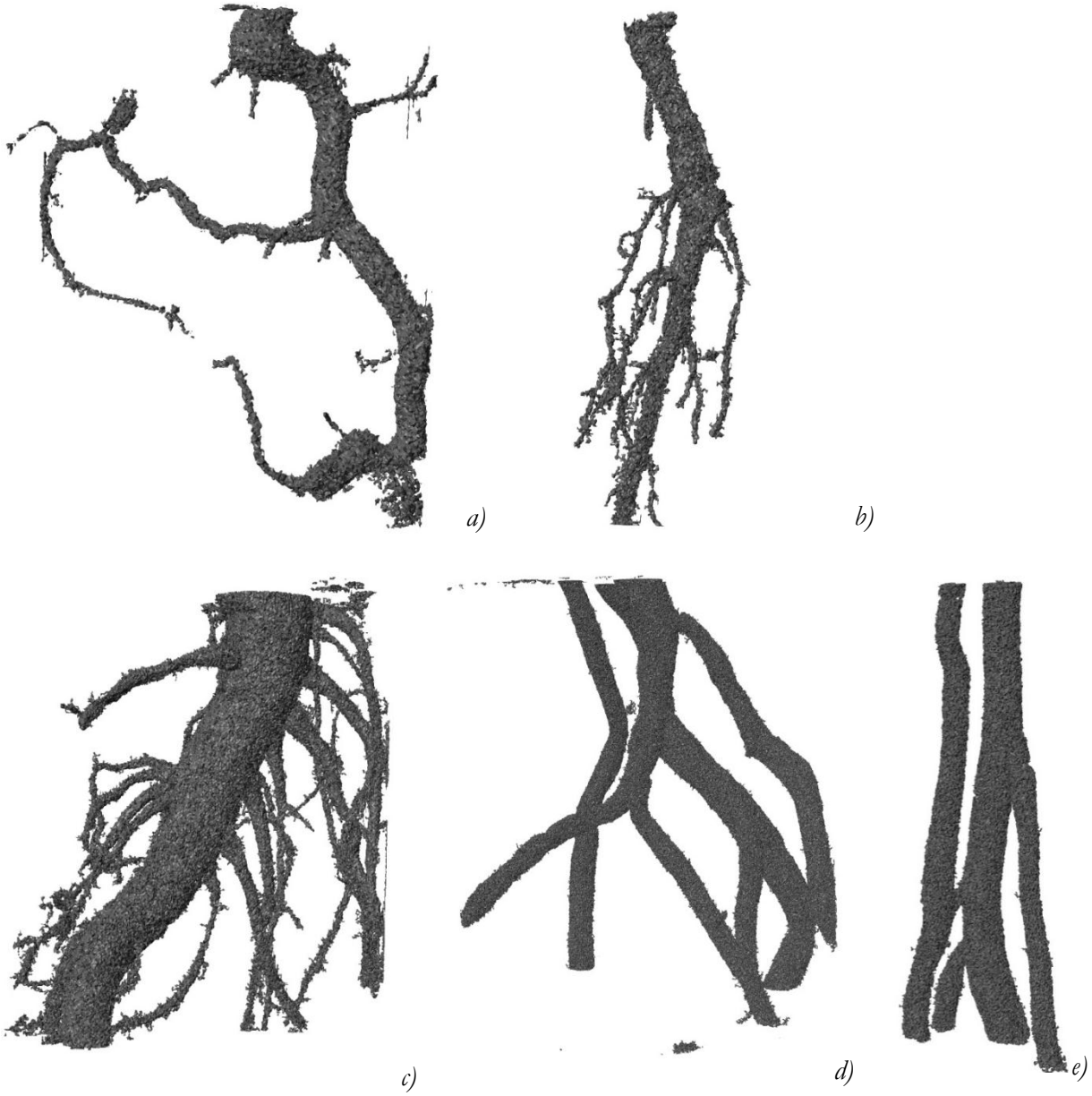

Figure 4 – Segmented root structures, obtained via CT scan techniques

The computational representations of the five plant root structures are presented in Figures 4a to 4e, where the data presented can bwas formulated through the utilisation of the post-processing program *ScanIP*. This program works to isolate the root zone through threshold segmentation; a process whereby a chromatic range limitation is applied to each individual pixel, thus isolating all pixels within that range from the overall data set. In addition to the segmentation process, the post processing programme allows for the discretisation of the geometry via the application of a surface mesh. The internal meshing package is greatly beneficial in comparison to that of other meshing programmes, such as *Ansys Workbench*, due to its ability to introduce appropriate boundary conditions and the capability to control surface element quality, thus allowing for the establishment of an optimised mesh.

The topologies shown in Figures 4a to 4e can be seen to consist of a number of two dimensional elements that are connected to pixels within the specified chromatic threshold.

The structures presented in Figures 4b and 4c, for example can be seen to consist of 262,996 and 2,635,076 elements respectively. In order to successfully mesh these structures, a smoother must be applied to reduce the surface roughness of the models. The comparative effects of applying a smoother is therefore presented within Figure 5, wherein the smoothed structure is shown to have a reduced degree of detail, but a more applicable surface for the meshing process.

The key problems encountered during the preliminary study included that of difficulties during the soil particle segmentation process and the loss of topological data during the smoothing process. Specifically, the soil particles within the sample were shown to have a similar threshold density to that of the root topology and thus some detail was lost from the soil particle geometry. This problem was, however, overcome through the utilisation of a different segmentation technique, wherein all grey scale particles connected to a selected particle could be sectioned. The second problem was overcome through the repetitive application of a significantly lower smoothing level. This ensured that the majority of the topology remained, but the faces of the root were significantly smoothed. Overall, the models presented show a high level of topological detail and can be seen to be an applicable to CFD modelling programs, such as that of *Ansys Fluent*, thus making CT modelling an ideal process for analysing root branches on a micro-scale level.

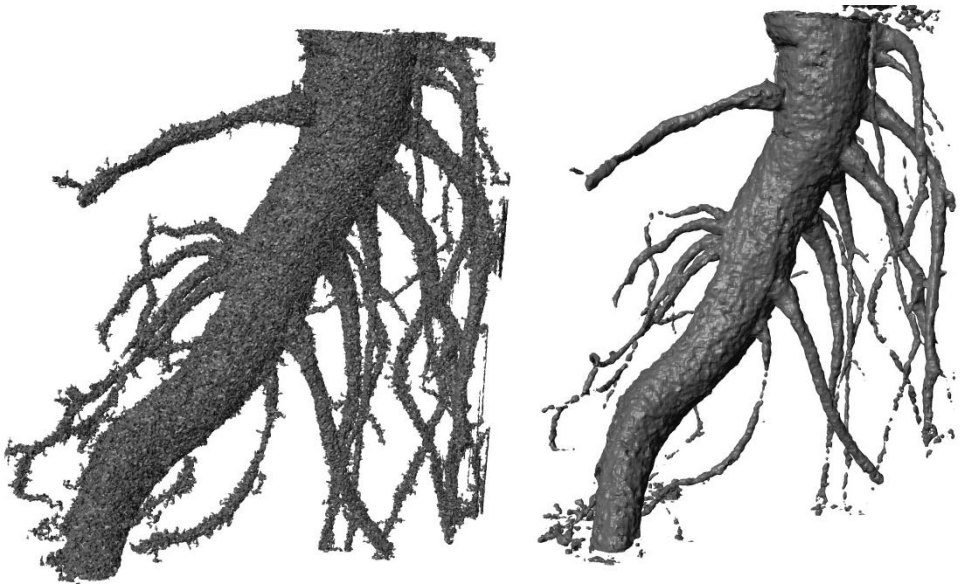

Figure 5 a) Surface topology of sample C without surface smoothing filter applied
b) Surface topology of sample C with smoothing filter applied

2.4 Root Branch Model

The plant selection process is an important aspect within the design of the *Hydro Filterra*^{TM} system, since the characteristics of the biological system can affect the total level of nutrient and fluid absorption, as previously discussed. The plant selection process entails an assessment of the system's maximum height, flowering and sunlight requirements, as well as taking into consideration the level of maintenance that is necessary to keep the system alive (Plant Selection Guide for Storm Water Bioretention Planters). This ensures that there is minimal effect upon ground cover and that the rooting system is diverse enough to occupy a suitable volume of soil, without being too invasive.

Taking into account these criteria, the plant species *Malus Evereste,* or the 'crab apple' tree, was chosen from the design guide by the experimental team as a suitable experimental focus and is to be used within work by J. Please and L. Whitehurst. The crab apple tree is a deciduous tree that can grow to heights of over 1.5m and can be seen to be species that thrives in well drained soils. In addition, the tree species selected has been identified as a species that is used within current *Hydro Filterra*^{TM} systems.

The root branch structure under investigation can be seen to be that of a first order root stem which has been extracted from the root architecture of the crab apple tree. The sample is presented within Figure 6, where the defined region is the region implemented into the computational model. The diameter of the main stem was identified as 6.24mm and the total length of the sample was measured as 93.61mm. The vertical distance between the proximal and distal ends of the segment was identified as 71.85mm and the soil structure surrounding the root topology was that of the *Hydro Filterra*^{TM} soil composition being investigated by L. Whitehurst.

The key offshoot branches presented within *region A* were found to have comparatively larger diameters than those of the offshoot branches seen further down the sample and therefore were identified as the most important offshoots to model. In addition, one of the offshoots can be seen to have an open distal end, thus allowing for an examination of the effects of the root tip geometry upon total absorption. *Region A* was therefore defined as the critical zone to analyse via micro CT techniques.

The computational representation of *Region A* is presented in Figure 6, wherein the two key offshoot branches have been segmented separately from that of the main stem. Both the soil particles and the root structures have also been smoothed appropriately to allow for the meshing process. In order to minimise computer power consumption, *Region A* was refined further, whilst still encapsulating the important topological features of the offshoots. This zone has been defined as *Region B*. Within *Region B*, the main stem is clearly visible as the green structure, whilst the blue offshoot, considered as the *Central Offshoot,* can be seen to have a larger diameter than that of the *Side Offshoot,* which is highlighted in yellow. A key point to note would be that of the formation of a root tip at the end of the *Central Offshoot*.

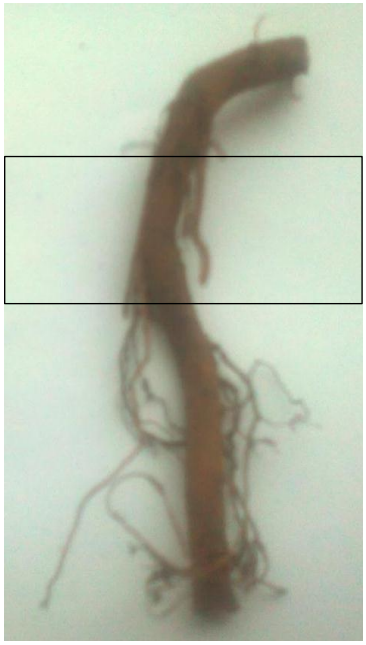

Region A: Zone selected for computational analysis.

Figure 6 – First order root branch extracted from Malus Evereste with Region A *section*

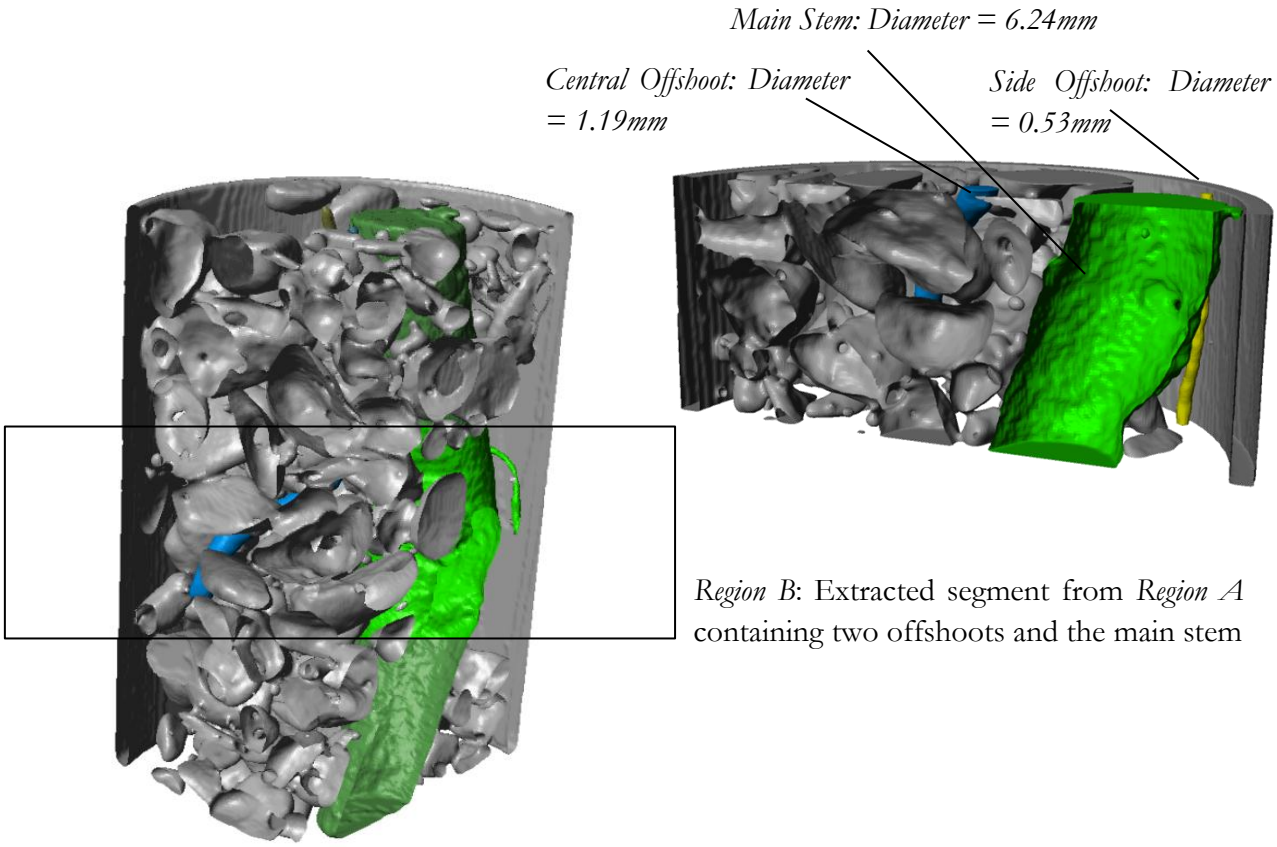

Figure 7 – Composition of Region A, established through CT results. Region B is a section of Region A

A comparison of the surface topology to that of the *Fluent* mesh is presented in Figure 8 in order to demonstrate its quality. Overall, *Region A* can be seen to consist of 3.6 million hexahedral cells and a total of 13.8 million tetrahedral cells. In contrast, Region B can be seen to consist of a total of 3.5 million cells. This is primarily due to the retained complexity of the geometry subsequent to the smoothing process. The total mesh is considered to be an accurate representation of the topology since the average cell volume ($1.4x10^{-9}m^3$) allows for the encapsulation of all changes in geometry without the loss of data and the system can be seen to contain no highly skewed cells. Additionally, increased mesh refinement will sufficiently affect computational demand and drastically increase simulation time.

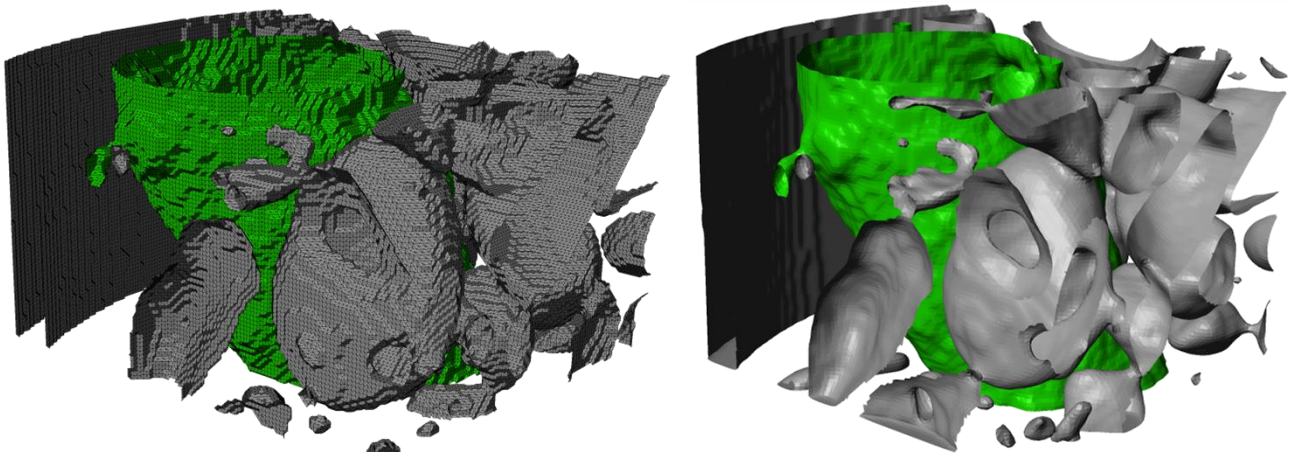

Figure 8 – Cross-section region highlighting the differences in quality between the CT surface topology and the discretised mesh

3.0 Macro Scale Modelling of Plant Root Architecture

3.1 Soil-Water Uptake by Plant Root Architecture

The consideration of soil water absorption on the macro-scale involves the application of a standard absorption characteristic to a global model. It differs significantly from that of micro-scale modelling in that the root architecture model is considered as a whole and does not apply specific characteristics to each of the root branches. The key benefits of modelling the system on a macro-scale can be seen to include that of gaining a better understanding of the effects of root architecture upon the flow at each layer of the soil region and allowing for the establishment of a global absorption parameter that will affect the fluid flux at the outlet of the bioretention system. In this section, a global root architecture model is devised and methodology is presented for deriving a global absorption parameter, which can be seen to be based upon the climatic data of the surrounding area and the geometry of the tree system above the soil layer.

The primary method of modelling root systems on the macro-scale level involves the application of a volumetric sink term to the equations that model the flow of water through a soil region. When considering the flux of fluid across an unsaturated soil region, one can use Darcy's law to relate the volumetric flux to that of the pressure drop across the system:

$$Q = -k(\theta)A_s \frac{dH}{dZ} \tag{3.1}$$

Where Q [m^3s^{-1}] is the change in volumetric flow rate across the soil, k [ms^{-1}] is the hydraulic conductivity of the soil, A_s [m^2] is the flow area, H is the hydraulic head, θ [m^3] is the volumetric soil water content and z [m] is the vertical position from the soil surface where the downward direction is considered positive.

By applying the continuity equation for soil water movement and representing the uptake of fluid by the roots as a sink term, F, one can establish the time rate of change of soil water content (equation 3.2). This allows for the derivation of the Richards Equations (Richards 1931), which characterises the movement of water in unsaturated non-swelling soils in terms of the temporal changes in soil water content.

$$\frac{d\theta}{dt} = -\frac{dq}{dz} - F(h) \tag{3.2}$$

$$\frac{d\theta}{dt} = \frac{d}{dz}\left[k(\theta)A_s \frac{dH}{dZ}\right] - F(h) \tag{3.3}$$

The sink term, F(h) [m^3s^{-1}], accounts for the total volume of water extracted by the root medium from the total soil water volume per unit time. In a number of studies, such as within work carried out by Simunek and Hopmans (2008), Feddes et al. (1976) and Wilderotter (2001), the sink term is characterised as the overall plant transpiration rate, which acts as the main driving force for soil-water uptake.

The sink term applied to the transport equation denotes the total volume of soil water absorbed by the entire root system per unit time. It therefore stands that the total volumetric

water uptake rate by the root structure equals that of the volumetric expenditure rate of the plant. Thus the soil water uptake rate can be seen to be dependent upon the evapotranspiration rate and the surrounding climatic conditions. The sink term can be parameterised through the use of the Penman Monteith equation (Monteith 1965), as used by the Food and Agriculture Organization (FAO) of the United Nations to predict crop water evapotranspiration levels (Allen et al. 1998). The Penman Monteith equation presents the entire evaporating surface as a single "big leaf" with two defining parameters. The first defines the atmospheric demand surrounding the surface and the second defines the biological characteristics of the plant.

$$ET_0 = \frac{\Delta(R_n - G) + 86400\ \rho_a\ C_p[\frac{e_a - e_d}{r_a}]}{\left[\Delta + \gamma\left(1 + \frac{r_c}{r_a}\right)\right]\lambda} \qquad (3.4)$$

Where ET_0 [$m^3\ s^{-1}$] refers to the time dependant changes in volumetric water content evaporating from the defined surface, Δ [$kg\ K^{-1}\ m^{-1}\ s^{-2}$] is the rate of change of saturation specific humidity with air temperature, Rn [$MJ\ m^{-2}\ s^{-1}$] is the net irradiance, Cp is the specific heat capacity of air, ρ_a [$kg\ m^{-3}$] is the density of air and δe is the vapour pressure deficit or evaporation rate at specific humidity. The parameters g_a and g_s refer to the conductivity of air (atmospheric conductance) and conductivity of the stomata (surface conductance) respectively and γ refers to the psychometric constant (~0.066 KPa $°C^{-1}$) (Howell et al. 2006).

The majority of parameters incorporated within the Penman Monteith equation are obtainable via an analysis of the climatic conditions surrounding the plant system, suggesting that only a small amount of experimental analysis is required. Several of the values, such as atmospheric temperature, net irradiance and humidity, can be seen to change both seasonally and/or hourly and therefore require further equations to define the evapotranspiration rate at specific time periods or are condensed into daily averages. In addition, the conductivity of the stomata, g_s, and the conductivity of air, g_a, can be seen to be very sensitive to temperature related changes and therefore can be modelled as inversely proportional to the parameter's resistance to change. Details of the derived parameters presented in equation (3.4) can be found within Section 8.2 of the Appendix.

3.2 Root Architecture Modelling

The process of constructing plant root models has been conducted in numerous different ways over the past years, where the most effective method can be seen to be that of considering the system as being fractal in nature (Liddell and Hansen 1992). Alternatively, one can utilise nodal positioning methods to determine the overall structure of the root system (T N Brown et al. 1996).

The system presented in Figure 9 is a computational representation of a root architecture system which was constructed using the modelling program *Solidworks 2011*. The model is based upon the principals of Lindenmayer systems (L-systems), which use production rules and an initial parameter to define a fractal network. Following with these systems, the main stem branch was set to branch into two offshoot branches that differ in diameter by a factor of 3. In addition, a random function for the branch angle was implemented at each offshoot position in order to integrate an aspect of stochastic evolution into the model.

It is important to note that the system can be constructed using the mathematical applications of *Solidworks* and the L-system technique, but, due to time constraints and the complexity of such an operation, the model can be seen to have been constructed simply through following with the production rule presented. In addition, a key observation to note would be that the system is considered to be completely developed and therefore the effects of growth are to be neglected.

A key aspect of the model presented is that of the importance of root branch order. The geometry presented in Figure 9 shows the divergence of a 24mm diameter stem into that of two 6mm stems and a 12mm stem. The 12mm stem was considered to be first order, whilst the offshoots of the smaller diameter branches were considered to be of second order. Any subsequent offshoots of these branches are deemed to increase in order accordingly. When considering root branches as individual cases, the order of the branch is likely to affect the hydraulic conductivity of the structure. This has been incorporated into the macro-scale model in terms of changes in branch diameter, which will bring about differences in velocity across the boundary, given a global volumetric flux parameter.

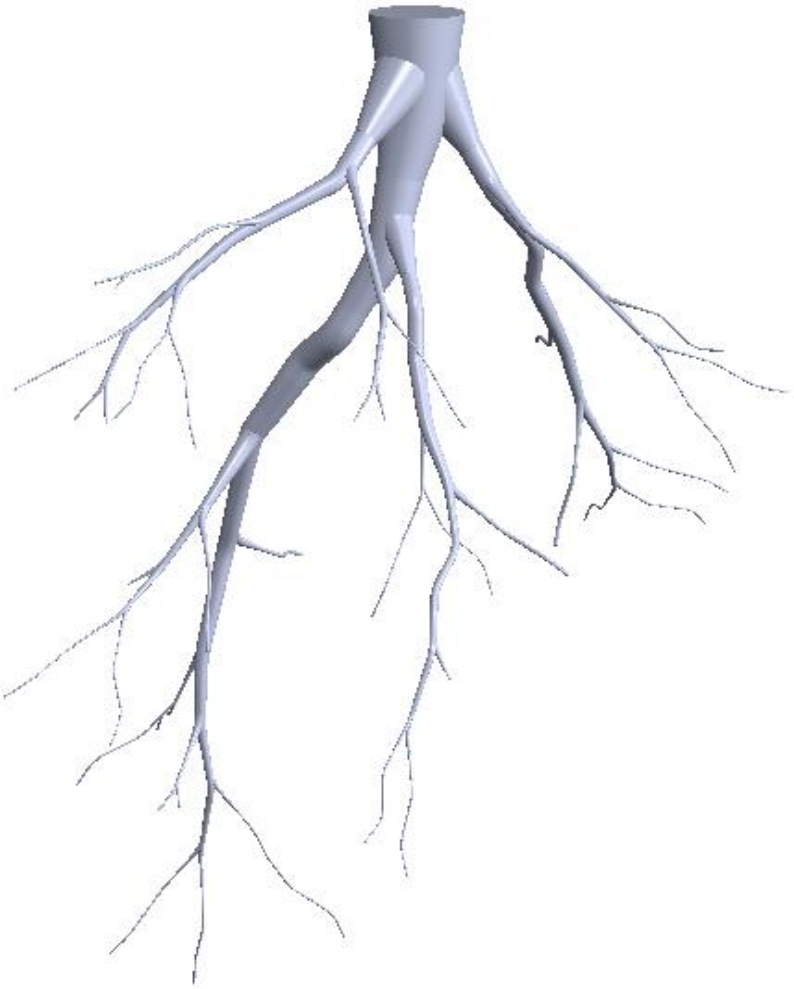

Figure 9 – Computational model of a plant root system

3.3 Macro-Scale Computational Modelling

The computational modelling programme OpenFOAM 2.0.1 is an extensive finite element package capable of modelling complex fluid flows that may involve chemical reactions, turbulent formations or heat transfer processes, as well as having the competence to analyse solid dynamics and electromagnetics problems (OpenFOAM user manual). It incorporates a range of features that can enhance meshing capabilities, improve post processing visualisation and allow for the introduction of explicit boundary conditions. Thus, OpenFOAM was considered to be an ideal CFD modelling program due to its advanced meshing capabilities and its ability to integrate a high level of detail into that of the case setup. This can be seen to be of great importance when considering the application of permeable boundary conditions and the discretisation of a complex structure, such as that of the root architecture model presented.

The overall case setup process can be seen to consist of establishing a suitable representation of a porous region surrounding that of the root architecture, followed by the subsequently extraction of the root architecture model (Figure 9) from that region. The porous region of the *Hydro Filterra*^{TM} system can be accurately represented through the implementation of the case file, *porousZones*, which works to apply a pressure drop across a specific region of the control domain, in accordance with Darcy's Law. The *porousZones* function can be seen to apply a sink term, S_i, to the Navier Stokes equation for incompressible flow, before integrating the time derivative over a discretised control domain. The sink term, S_i, uses the Darcy Forchheimer law (Equation 3.5) to incorporate the pressure drop across the region and can be seen to be dependent upon the combination of a viscous and an inertial loss term:

$$S_i = -\left(\mu d + \frac{1}{2}\rho|U_{jj}|f\right)U_i \qquad (3.5)$$

Where the scalars *d* and *f* represent the viscous resistance parameter and the inertial resistance parameter respectively, μ [Pa s] is the dynamic viscosity of the fluid, U[ms^{-1}] is the fluid velocity and ρ [kg m^{-3}] is the density of the fluid.

```
soil
{
    coordinateSystem
    {
        e1  (0 0 1);
        e2  (1 0 0);
    }

    Darcy
    {
        d   d [0 -2 0 0 0 0 0] (1.42e9 1.42e9 1.42e9);
        f   f [0 -1 0 0 0 0 0] (9.86e4 9.86e4 9.86e4);
    }
}

gravel
{
    coordinateSystem
    {
        e1  (0 0 -1);
        e2  (1 0 0);
    }

    Darcy
    {
        d   d [0 -2 0 0 0 0 0] (2.2e7 2.2e7 2.2e7);
        f   f [0 -1 0 0 0 0 0] (4.34e3 4.34e3 4.34e3);
    }
}
```

Figure 10 – Data contained within the case file porousZones

The *porousZones* case file setup is presented in Figure 10, wherein the direction of resistive force is defined by the two vector coordinates, *e1* and *e2*. The third vector is created orthogonally to these coordinates and is used collectively to define the direction of porosity. The resistance parameters d and f also rely on the coordinate system and are set according to the units table presented. For the setup above, the parameters *d* and *f* were established through the utilisation of the Ergun Equation, which can be used to assess the friction factor of a packed column with respect to the Reynolds number (Akgiray et al. 2001.) The parameters presented in Equations (3.7) and (3.8) have been computationally tested within work by S. Pavey, which contrasts the presented values with that of the experimental work carried out by J. Please. Thus, the application of the Ergun Equation is considered to be a valid method of derivation for the parameters for viscous and inertial loss.

$$\frac{\Delta P}{L} = \frac{150\,\mu\,(1-\varepsilon)^2}{{D_p}^2\varepsilon^2}\,U^2 + \frac{1}{2}\rho\,\frac{3.5\,(1-\varepsilon)}{D_p\,\varepsilon^3}\,U \qquad (3.6)$$

$$d = \frac{150(1-\varepsilon)^2}{{D_p}^2\varepsilon^2} \qquad (3.7)$$

$$f = \frac{3.5\,(1-\varepsilon)}{D_p\,\varepsilon^3} \qquad (3.8)$$

Where ΔP [Pa] is the change in pressure through the system, which is of length, L [m], d_p[m] is the average particle diameter and ε is the void fraction.

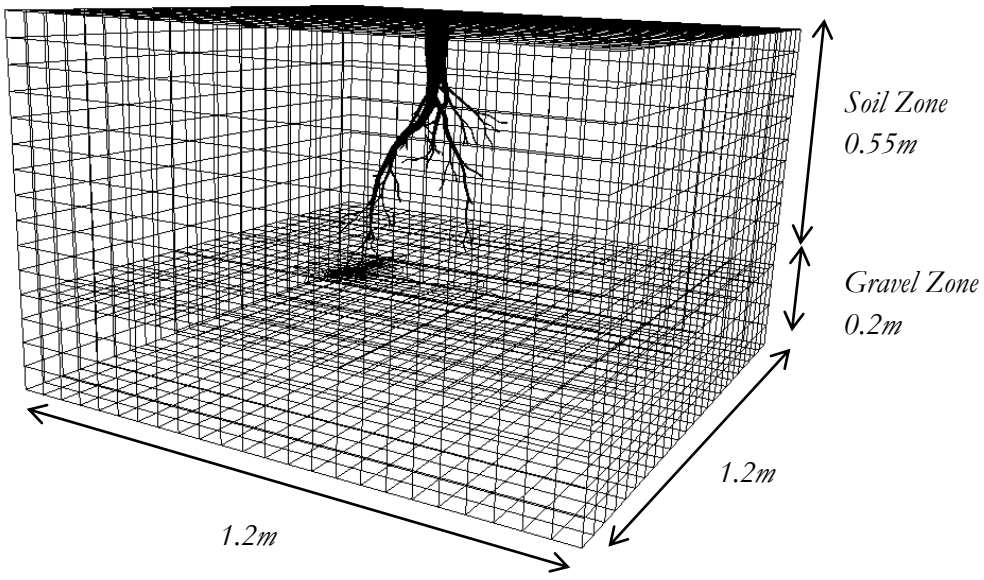

Figure 11 – schematic of the control volume with incorporated porous regions

Subsequent to the establishment of the two porous regions, the macro-scale root architecture topology was extracted from the control domain. The extraction process involved the utilisation of the *snappyHexMesh* function within OpenFOAM, since this was deemed to be the most appropriate meshing package for a complex model such as this. The *snappyHexMesh* process works in two key stages, the first of which involves the process of refining the hexahedral cells of the control domain into that of much smaller cells, where the cells are

selected if more than 50% of their volume contains the presented geometry. The following stage can be seen to consist of mapping the refined cell vertex points to that of the root surface, thus smoothing the surface topology and producing a valid mesh. The formulated mesh is presented within Figure 11, where the control domain can be seen to consist of a total number of 555,826 cells. The data also presents the porous regions *soil* and *gravel*, which are identifiable within the *porousZones* case file. The results of the mesh refinement process can be identified within Results and Discussion section (*Section 4.2.1*).

When considering the mesh presented, one can identify two key areas of geometrical complexity. These can be seen to be that of the positions of branch connection and the extremely small diameter of the highest order branches. The data shown in Figure 12 illustrates the requirement for a higher mesh density at the positions of branching and a significant level of cell refinement in areas of root tip geometry, in order to prevent the loss of topological data. However, a key disadvantage of significantly reducing the cell size in these regions can be seen to be that of an increase in the computational demand and an extensive simulation time.

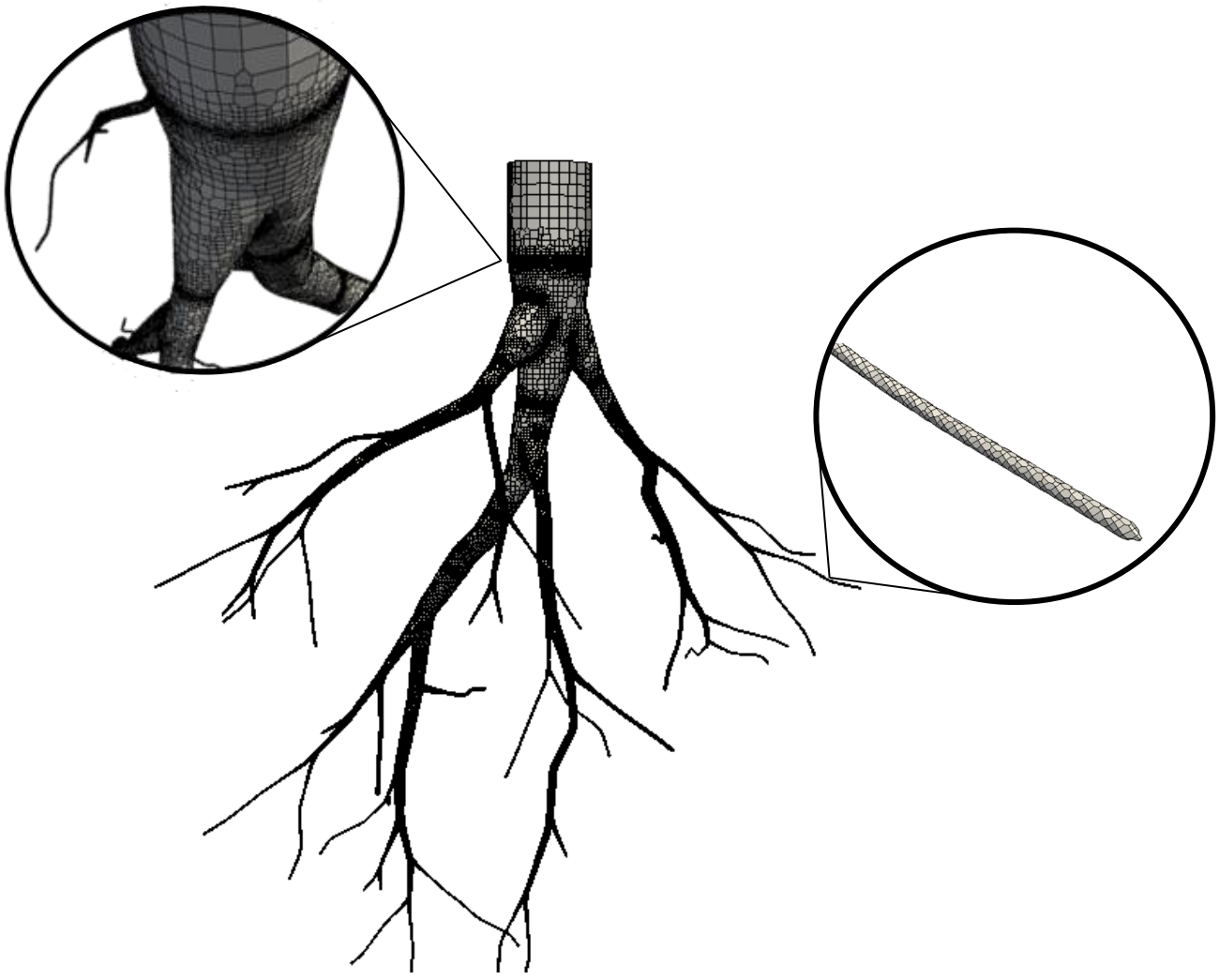

Figure 12 – Computational mesh of the root architecture model

In order to ensure the accuracy of the results, a k-epsilon turbulence model was incorporated into the case setup. Primarily, the effects of turbulence within the case were

expected to be negligible. However, the inclusion of a turbulence model was deemed necessary in order to cover any possible turbulent effects caused by the root structure. The k-ε model was chosen due to its flexibility. The model is considered to be applicable to a number of situations and is only heavily affected by cases that consider high levels of fluid compressibility, such as that of centrifugal compressor systems. The key parameters included within the model were those of the turbulent kinetic energy parameter, k [m^2s^{-3}], and the turbulent energy dissipation parameter, ε [m^2s^{-3}], which were approximated as:

$$k = \frac{2}{3}(U\,Ti)^2 = 1.951x10^{-8}\,m^2s^{-3} \qquad (3.9)$$

$$\varepsilon = C\mu^{3/4}\frac{k^{3/2}}{0.07L} = 7.569x10^{-12}\,m^2s^{-3} \qquad (3.10)$$

$$I = 0.16Re^{-\frac{1}{8}} = 0.326\,\% \qquad (3.11)$$

Where Cμ is a model constant related to wall boundary conditions (Cμ=0.09), Re is the Reynolds number, L [m] is the characteristic length and I [%] is the turbulent intensity parameter.

4.0 Results and Discussion

4.1 Results of the Micro Scale Investigation

4.1.1 Radial Conductivity

The results of the micro-scale computational assessment are presented in Figures 14 to 17, wherein the changes in radial flow rate with depth have been compared to that of the changes in total pressure with depth for ten key data lines. The data presented was extracted from the *Fluent* simulation via the implementation of data lines positioned at distances of 1mm from the surfaces of each root branch, as illustrated within Figure 13. This method allows for an assessment of the radial driving force in multiple locations and thus the establishment of a more accurate radial conductivity parameter. The internal pressure of each root branch was set as p_r=0 and the radial conductivity, k_r, of each structure was considered to be constant.

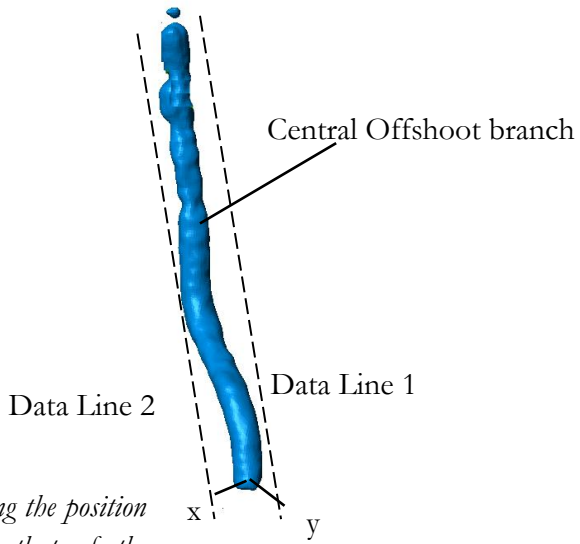

Figure 13 – Schematic illustrating the position of the data lines surrounding that of the Central Offshoot branch

The key findings of the presented data can be seen to include that of differences in the magnitude of radial conductivity with increased root diameter. Specifically, a significantly higher radial conductivity for the *Central Offshoot* can be identified in contrast to that of the *Side Offshoot*, where the radial conductivity, k_r, of the *Central Offshoot* can be identified as k_r=0.178ms^{-1}Pa^{-1}. This value is derived as an average of the four gradients shown in Figure 14. In comparison to this, the radial conductivity of the *Side Offshoot* was established as kr=0.104ms^{-1}Pa^{-1}. However, this magnitude can be seen to be highly skewed by the data set *Side Offshoot Line 1,* which may have been distorted by fluid moving into a branch section connected to the main stem, close to that of the data line. Thus, a more accurate value for the *Side Offshoot* branch would be k_r=0.0619 ms^{-1}Pa^{-1}, which does not take into account the skewed data.

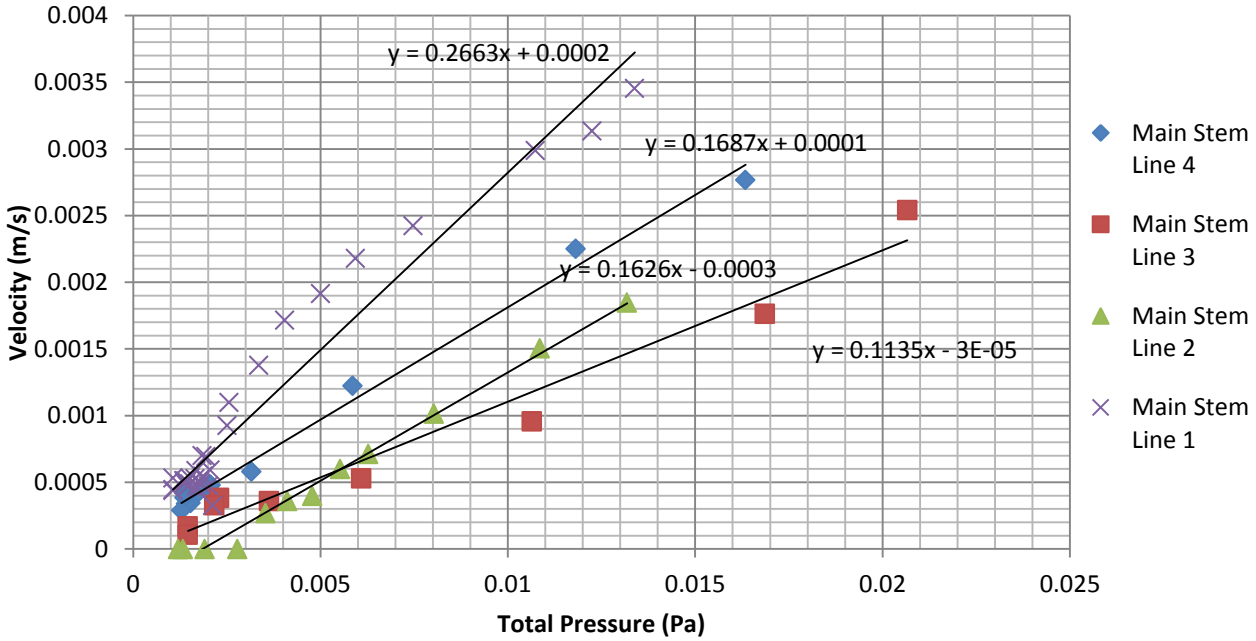

Figure 14 – Comparison of the changes in total fluid pressure with flow velocity across the boundary of the Central Offshoot branch

In contrast to the derived magnitudes of radial conductivity for the *Central Offshoot* and *Side Offshoot* structures, the radial conductivity of the *Main Stem* structure was calculated as kr=0.324ms^{-1}Pa^{-1}. This magnitude is a product of the main stem data lines 1, 3 and 5 presented in Figures 15 and 16. The data sets labelled 2 and 4 in Figures 15 and 16 are considered to contain anomalous data, which may have been affected by the movement of fluid into the *Side Offshoot* branch or the presence of a root structure within the immediate vicinity of data set 4. Overall, the radial conductivity for the *Main Stem* can be seen to be comparatively higher than that of the *Side Offshoot* and *Central Offshoot*, due to the major differences in diameter between the structures.

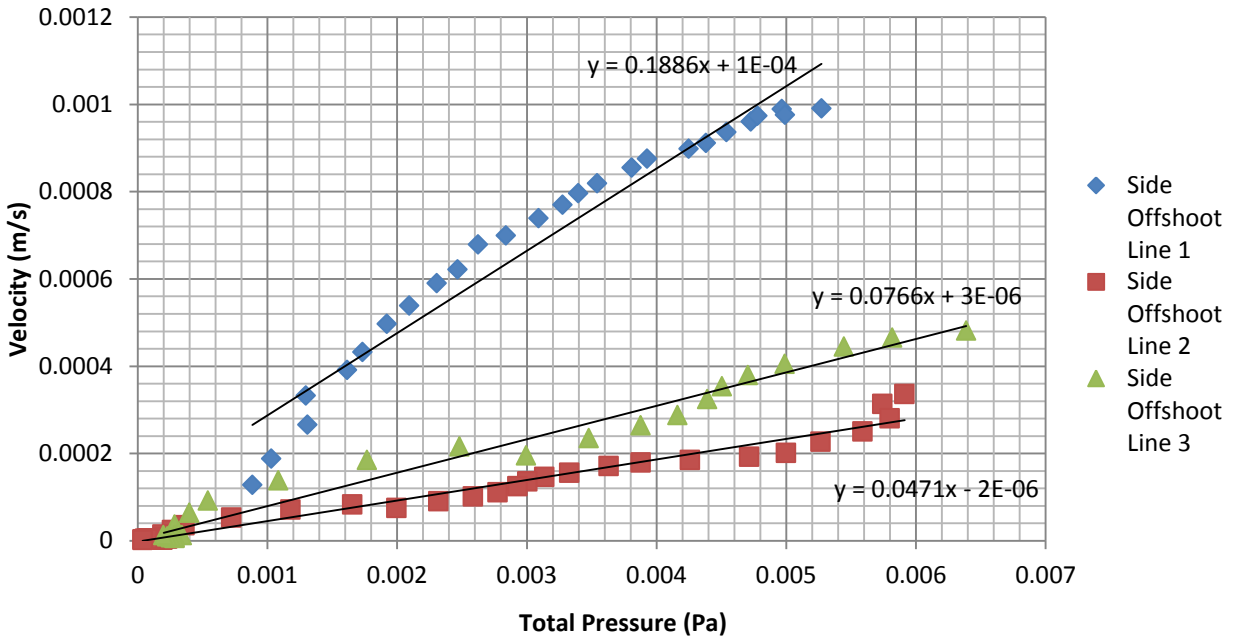

Figure 15 – Comparison of the changes in total fluid pressure with flow velocity across the boundary of the Side Offshoot branch

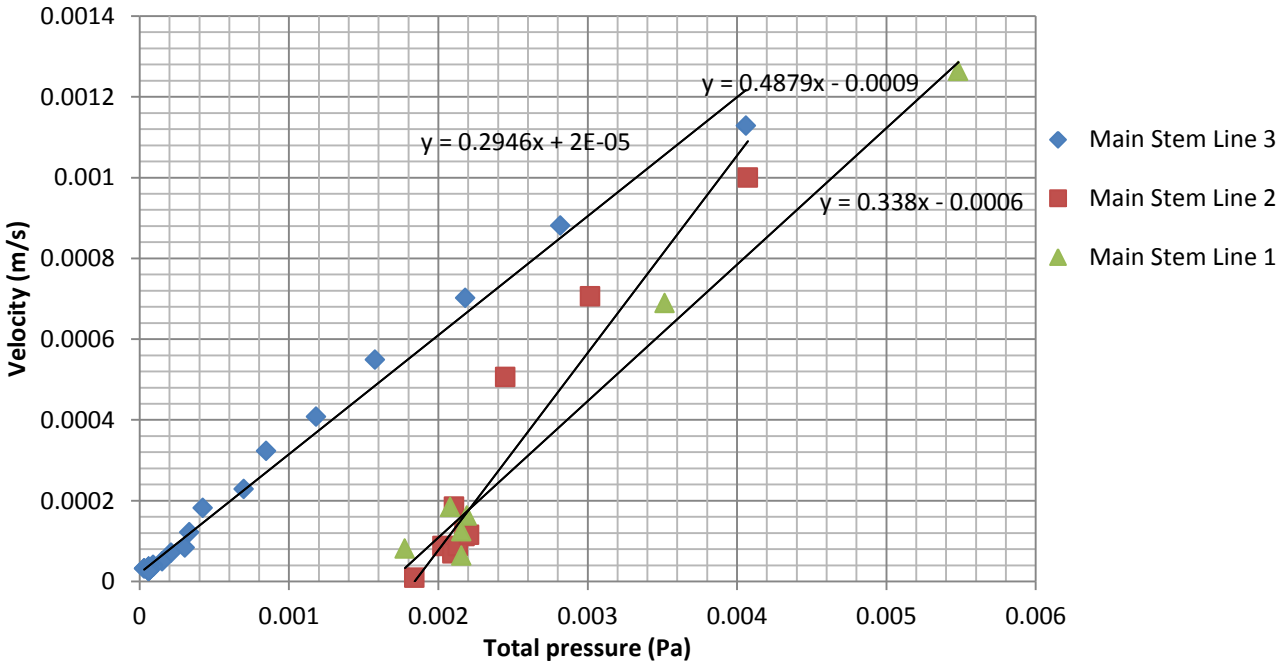

Figure 16 – Comparison of the changes in total fluid pressure with flow velocity across the boundary of the Main Stem branch

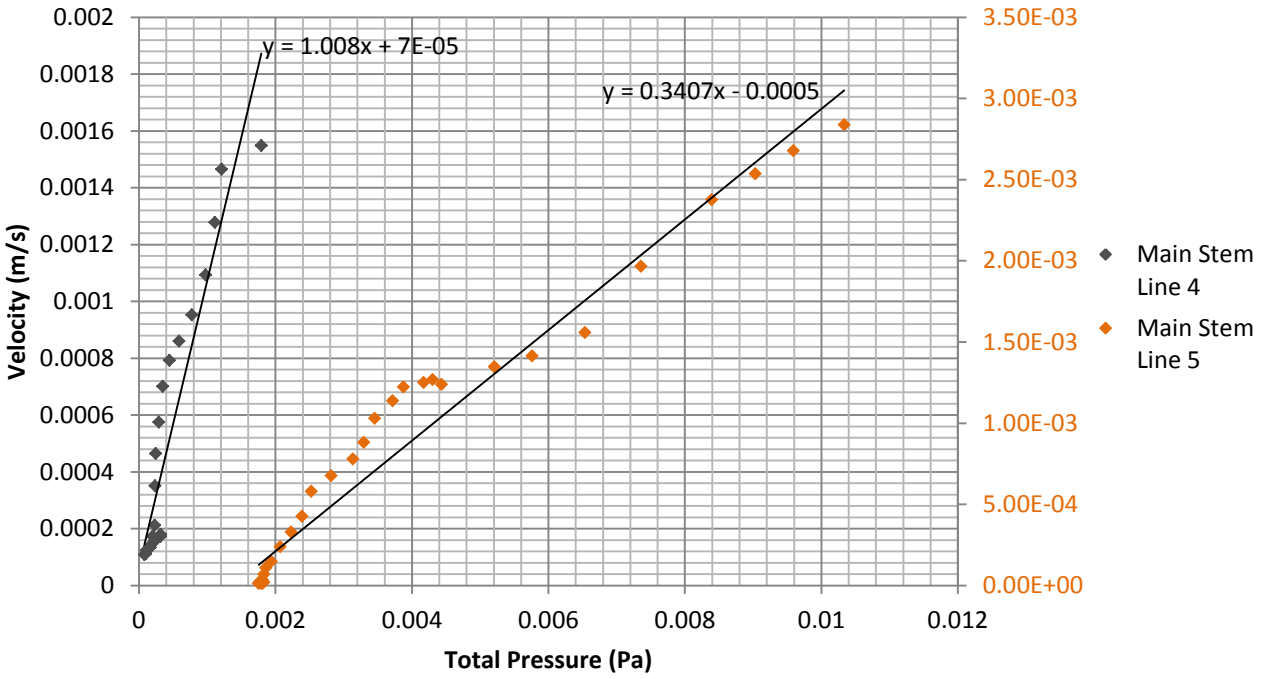

Figure 17 – Comparison the changes in total fluid pressure with flow velocity across the boundary of the Main Stem branch

The magnitudes of radial conductivity have been shown to increase with increased root diameter (Figure 18). This data can be seen to correlate to the experimental data presented by North and Nobel (North and Nobel 1995) which works to assess the hydraulic conductivity of a 3mm diameter root sample. The incorporated techniques involve the application of a controlled negative pressure to the inside of the sample and an investigation of the volumetric flow rate in the radial direction. The key results of the study present a sample hydraulic conductivity of 0.24 $ms^{-1}Pa^{-1}$. When considering the trend presented in Figure 18, one can identify that that a root diameter of x=3mm will bring about a radial hydraulic conductivity of 0.246 $ms^{-1}Pa^{-1}$, which can be seen to correlate with that of the experimental data. However, a key point to note is that of the effects of root tip geometry upon the magnitude of radial conductivity. Specifically, the experimental results of study show an increase in the radial conductivity from a magnitude by a magnitude of k_r=0.05 $ms^{-1}Pa^{-1}$ with the removal of the distal end seals, which have been incorporated to prevent conduction in the axial direction. This shows that the effects of root tip geometry can bring about changes in the magnitude of radial conductivity. Thus, the trend presented may be distorted by the presence of the root tip structure, such as that seen within the *Central Offshoot* branch.

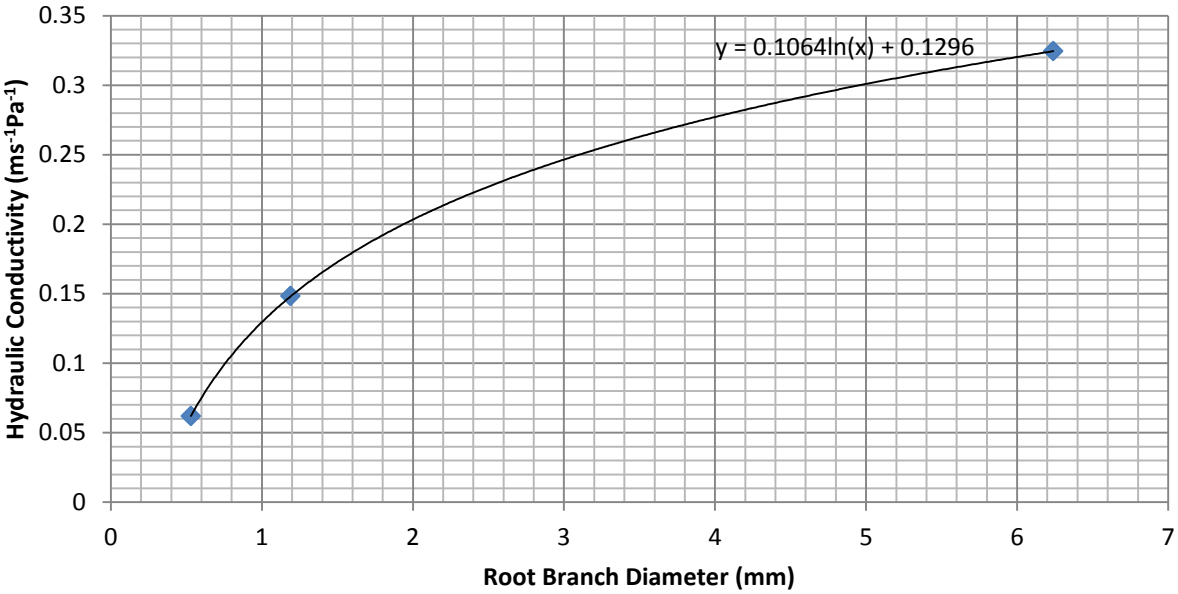

Figure 18– Graphical representation of the change in root hydraulic conductivity with increased root diameter

4.1.2 Axial Conductivity

The assessment of root branch conductivity is based upon the analysis of both the radial and axial hydraulic conductivity components. The data presented within Figure 19 shows the theoretical magnitudes of axial conductance for the root branches under investigation. In addition to the calculated magnitudes, the table contrasts the derived values with that of experimental data carried out by Frensch and Streudle (1989), which assesses changes in the hydraulic properties of maize roots with distance from the root tip. The study can be seen to incorporate the same methodology as that which is presented within Section 2.1 and can be considered to be an appropriate validation of the given values for axial and radial conductivity, due to the high level of experimental analysis within.

The key parameters contained within Figure 19 can be identified as those regarding the number of the metaxylem vessels and geometry of the vessels. These parameters are based upon the same work by Frensch and Streudle (1989), which implements fluorescence microscope data to visually analyse the structure of the root branch. A key observation to note would be that of the changes in the total number of early and late metaxylem vessels with root order, as these are the primary factors for assessing the axial conductivity of the system.

The results presented indicate that the radial hydraulic conductivity of root branch systems is significantly more important than that of the axial demand. In addition, the magnitudes of axial conductivity can be seen to be inversely proportional to that of the axial resistance to fluid uptake. Thus, for much thinner root branches and branches of lower order, the total volumetric uptake of fluid from the surrounding region can be seen to be greatly reduced due to an extensive resistance to axial flow. The primary factors that are shown to affect the axial conductivity can be seen to include that of the branch diameter and the total cross-sectional area. This is illustrated through a comparison of the *Central Offshoot* and *Side Offshoot* systems, wherein the axial conductivity can be seen to vary by two orders of magnitude, given an increase in diameter of 0.66mm. A final key observation to note would that of the independence of the results upon the length the branch. Experimental analysis of root branch

systems has shown that the axial conductivity parameter, k_z, is dependent upon the total number and diameter of the early metaxylem and protoxylem within a root branch. This can be seen to vary with respect to the cross-sectional area of the branch, thus neglecting the effects of xylem vessel length upon the degree of axial conductivity. The radial conductivity parameter, k_r, has, however, been proven to be highly dependent upon the radius and length of the branch.

The key limitations to the data presented can be seen to include that of assumptions for the total number and geometry of the xylem vessels within each branch. Specifically, the development of metaxylem vessels has been shown to be highly dependent upon the maturity of the root system, as well as its order (H D Hooker 1986). Therefore, since the axial conductivity parameter, k_z, varies with the fourth order of xylem radius, the results could be significantly affected. This has been highlighted by experimental work by Doussan et al. (2002), wherein the circular formation and radii of metaxylem vessels is revealed to be non-uniform through the cross-sectional area of the branch. In addition to this, the Hagen-Poisuelle pipe flow equation assumes a uniform cross section pipe without the inclusion of bends. Thus, the results may be affected by the bends within the root branches and changes in xylem vessel diameter with height, z. Nevertheless the results have been proven to be comparable to those of the experimental results and are considered to be unaffected by root branching regions, which have been shown to distort the total magnitude of axial conductivity.

	Main Stem	**Central Offshoot**	**Side Offshoot**	**Experimental Values (Frensch and Streudle 1989)**
Diameter (10^{-3} m)	6.23	1.19	0.53	3.00
Length (10^{-3} m)	10.01	6.82	10.01	50.00
Face Area (10^{-6} m^2)	30.55	1.12	0.22	7.07
Root Order	1	2	2	2
No. Early metaxylem elements per unit area	16.2	3	3	3
No. Late metaxylem elements per unit area	6.6	0.5	0.5	0.5
Early metaxylem diameter (μm)	27.4	27.4	27.4	27.4
Late metaxylem diameter (μm)	92.3	92.3	92.3	92.3
k_z ($m^4s^{-1}Pa^{-1}$)	$1.84x10^{-11}$	$2.94x10^{-15}$	$6.92x10^{-18}$	$4.22x10^{-14}$

Figure 19 – Comparison of the axial conductivity of the Main Stem, Central Offshoot and Side Offshoot branches to that of experimental data

4.1.3 Visual analysis

The velocity contour plots of several cross section planes are presented in Figures 20 to 22, where a schematic showing the specific positions of the planes is presented in figure 23. When considering the flow of fluid into that of the main stem, one can identify a large increase in flow velocity near the top of the root branch and a significantly lower flow velocity near the base of stem, as presented in Figure 20. Specifically, the flow at the top of the system is shown to be hindered by only a few small particles. However, when moving vertically, the flow can be seen to interact with much larger particles and thus a significant decrease in flow velocity is identifiable. Primarily, the larger soil particles will bring about a greater decrease in flow velocity due to a larger obstruction area, but the smaller particles will still induce changes in the flow velocity due to viscous shear stresses. The key implications of a changing flow velocity can be seen to include that of variations in the magnitude of total pressure within the external area, which can be seen to be based upon the components of the static and dynamic pressures. These changes will inevitably affect the radial driving force across the boundary of the root structure and therefore the radial conductivity of the root system. Thus, we can establish that the average particle size and void fraction are critical factors that can affect the radial conductivity of the root system since they govern the pressure gradient across the root boundary.

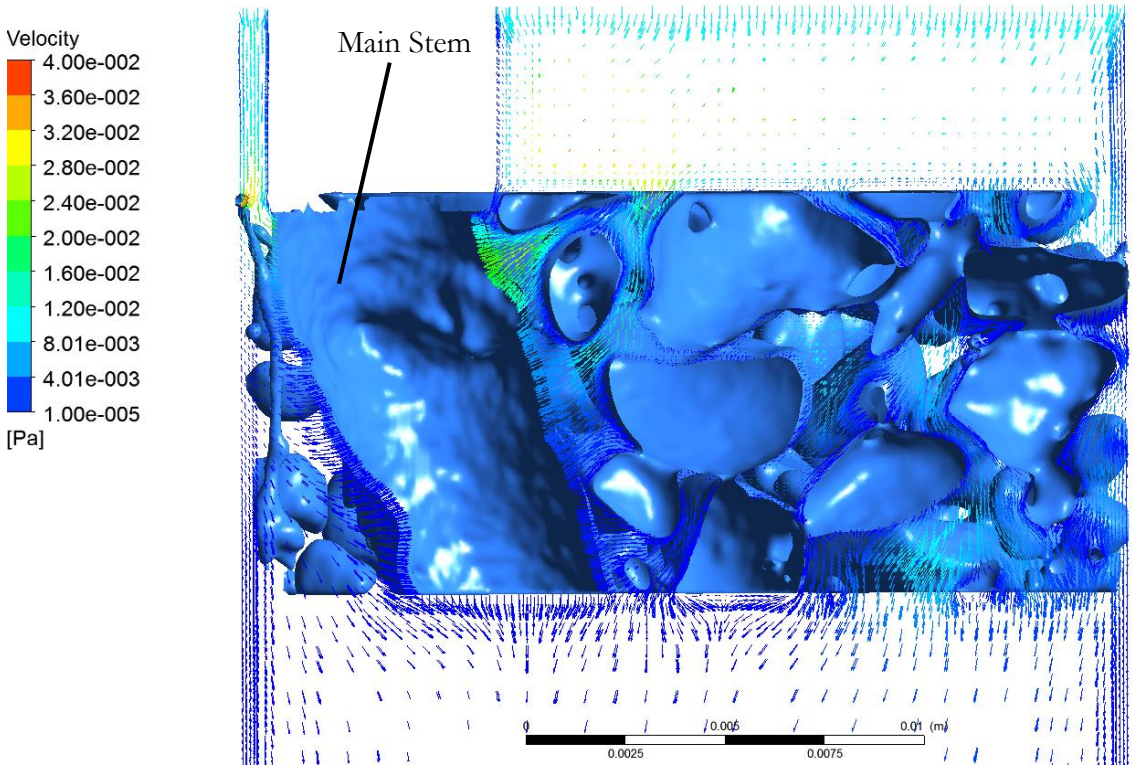

Figure 20 – Velocity contour plot of fluid moving through the root soil region Plane 1

When assessing the radial absorption characteristics of root structures, one must consider the effects of soil particle compaction within the immediate area of the structure. The data presented in Figures 20 and 22 shows a small gap between that of the root surface and that of the adjacent particles. This is particularly highlighted within Figure 20, wherein a large void space can be identified next to the *Main Stem* branch. This means that the movement of fluid is unrestricted within this area, thus presenting an aspect of the model that is considered to be

inaccurate with regards to that of a typical root soil system. Principally, the effects of soil compaction have been shown to affect the conductivity of the root system through an assessment of the changes in flow velocity across the boundary. However, work undertaken by L. Whitehurst and J. Please has shown that the movement of fluid through a porous medium, such as that of the soil structure presented, will bring about the removal of the much smaller particles and induce a greater level of soil particle compaction. Thus, the results of the simulation can be seen to be somewhat limited in that the effects of fluid movement upon changes in soil porosity have not been fully modelled.

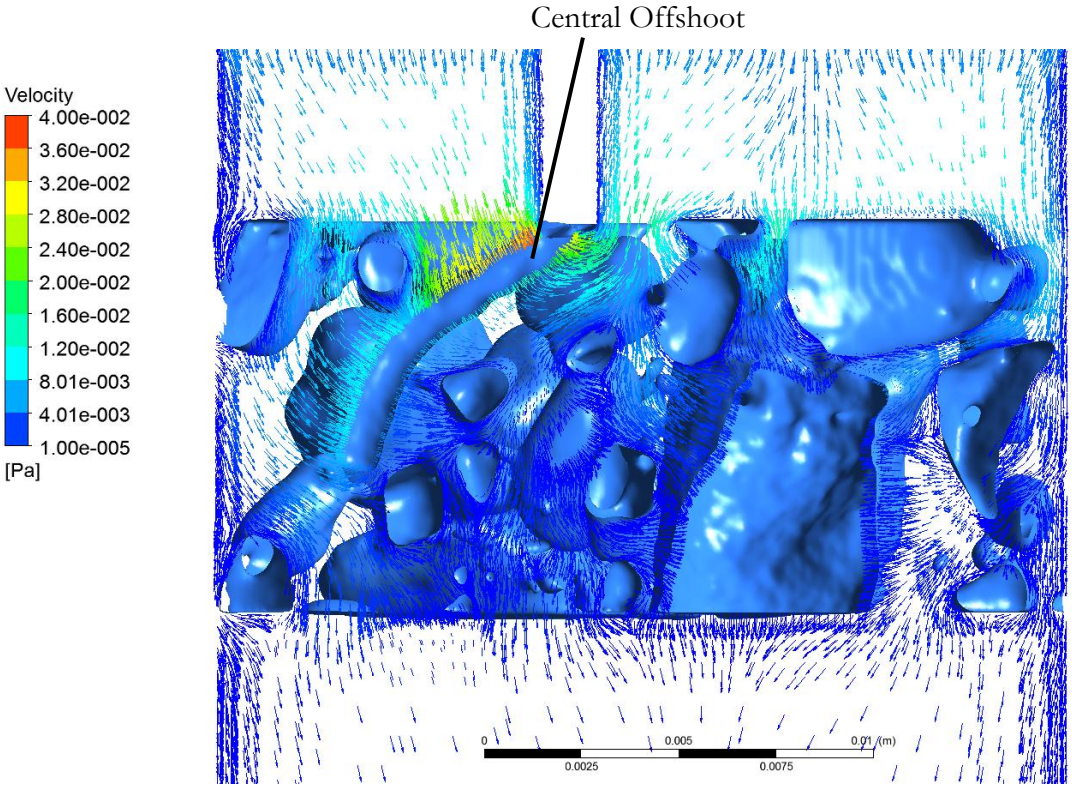

Figure 21– Velocity contour plot of fluid moving through the root soil region Plane 2

Figure 21 describes the movement of fluid through a soil region that is occupied by a root structure that incorporates a root tip. The resulting effects of the root tip geometry can be seen to include that of a greater redirection of fluid past the base of the structure and the movement of fluid in a direction opposite to that of the inlet velocity at the face of the tip. The limited degree of soil resistance and surplus effects of the root tip are shown to bring about a much higher magnitude of radial conductivity than that which is expected. However, the data is somewhat ambiguous as it incorporates the effects of the main stem on one side and that of an inaccurate representation of soil compaction on the other. In addition, the branch can be seen to exhibit a high degree of curvature, which results in a greater contact area with that of the free stream, thus skewing the magnitude of radial conductivity for the *Central Offshoot* structure. Nevertheless, an assessment of four data lines surrounding the branch has presented a suitable degree of coherence between the data sets and therefore the results are seen to carry some weight. In order to further assess the effects of root tip geometry upon the radial conductivity, one could apply the same techniques to an investigation of the flow regime surrounding several different root tip structures.

An important area of analysis is that of the key effects of root branching and structure proximity upon the nature of the flow regime. These aspects are both illustrated in Figure 22, wherein the observable cross section cuts through an offshoot of the *Main Stem* and incorporates the position of the *Side Offshoot* structure, which can be seen to be situated within the vicinity of the *Main Stem*. The results show a disproportionate level of fluid movement into that of the *Main Stem*, where a higher flow velocity can also be observed across the face of the boundary. It is therefore proposed that a root branch with a greater hydraulic conductivity will draw water away from that of a lower order branch, but will not prevent fluid from moving into the competing branch. This assessment follows with work undertaken by Molisch and Sachs (1983) which investigates the response of root systems to given stimuli. The study confirms that when two branches are competing, the branch which is of lower order will absorb fluid, but the volumetric flow rate will not be comparable to that of the higher order stem.

In addition to the effects of root branch competition upon the nature of the flow, the presence of a root branch node, or position of branching, has been proven to bring about increased absorption rates in contrast to that of the rest of the offshoot structure. This is a result of changes in the internal structure of the system, where the cortex region has been found to be decreased in thickness at the position of the joint (McCulley et al. 1993). Since the simulation does not consider the internal structure of the root branch, the changes in radial conductivity have not been identified. In addition, the results of the radial conductivity study regarding the *Main Stem* structure have not shown any consistently anomalous data at the position of the branch and the pressure field was found to be wholly predominantly unaffected at the position of branching.

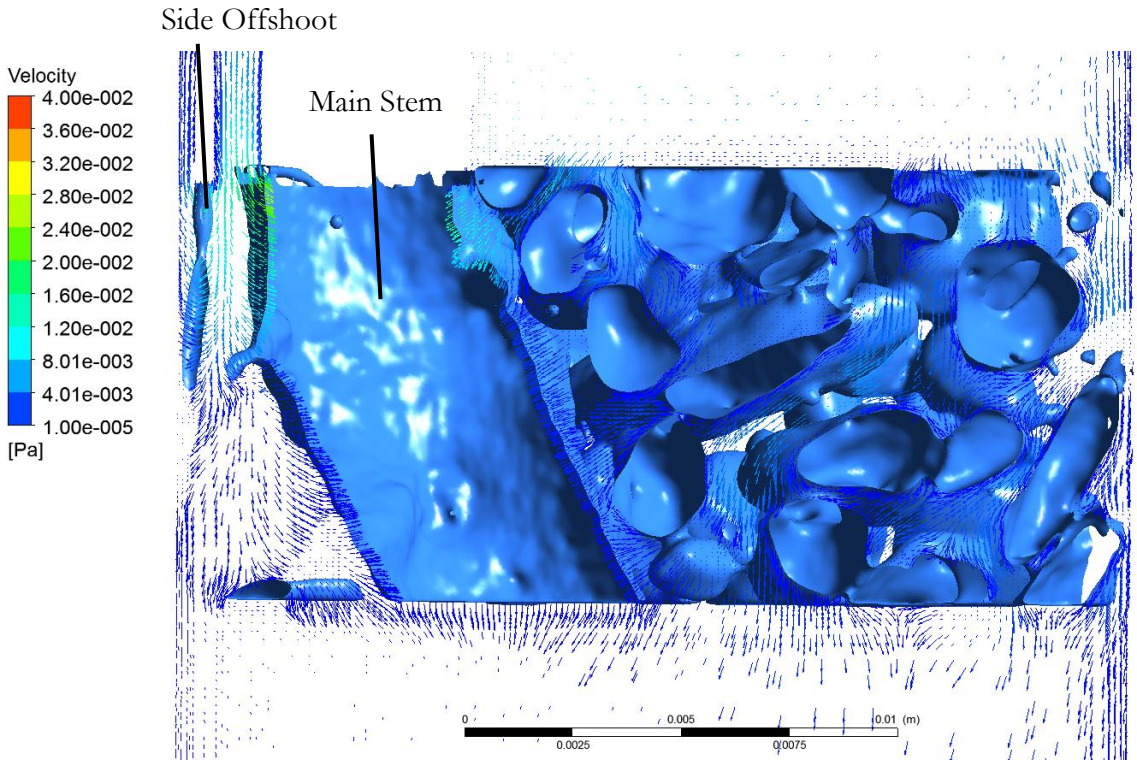

Figure 22 – Velocity contour plot of fluid moving through the root soil region Plane 1

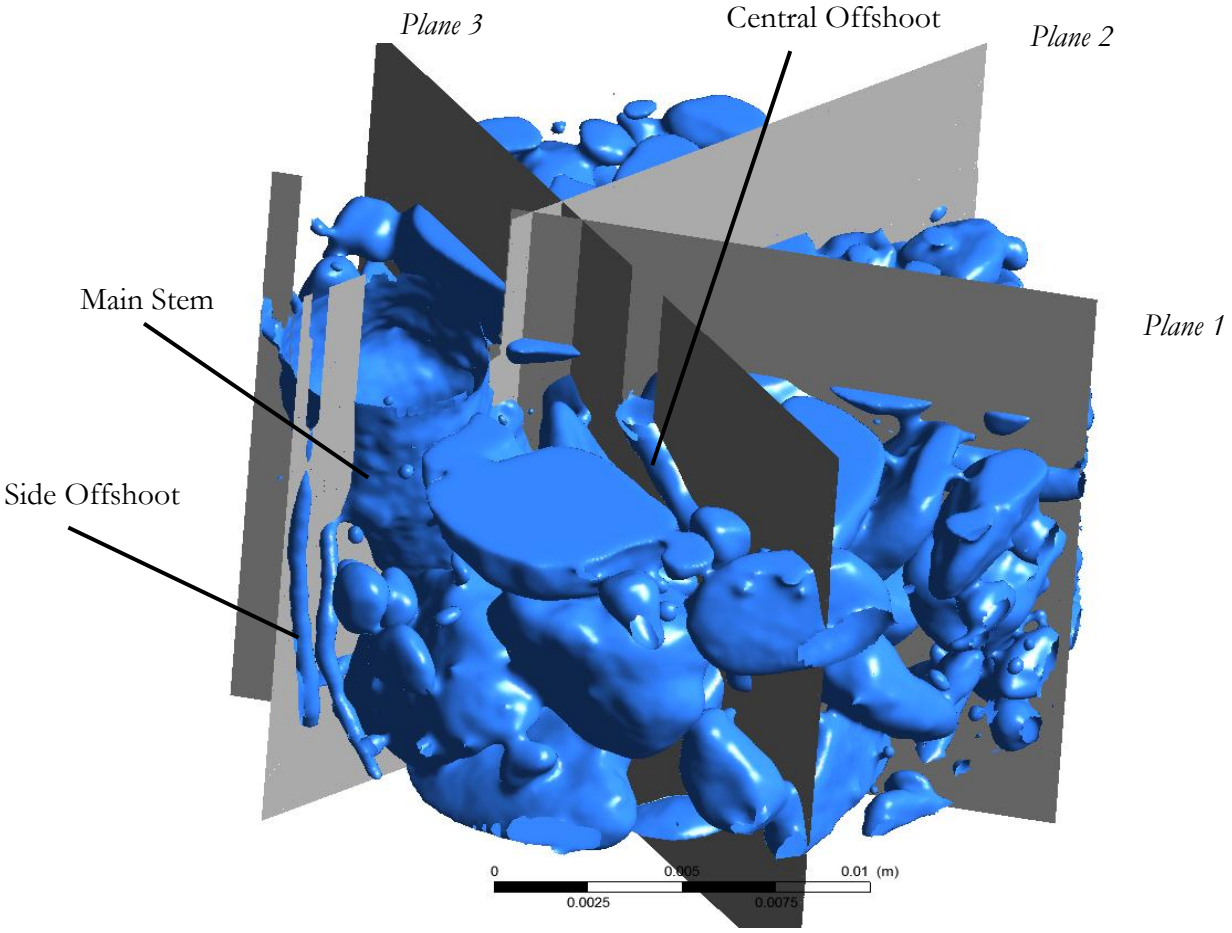

Figure 23 – Three dimensional representation of the root soil zone with incorporated analysis planes.

4.2 Results of the Macro Scale Investigation

4.2.1 Mesh Refinement

The mesh refinement process can be seen to be a critical stage of any CFD simulation since it defines the level of accuracy within the results. It is important that the model discretisation process implements an awareness of the computational requirements and the overall mesh time, in order to allow for the production of an optimised mesh. The results presented in Figure 24 show the convergence of the mesh towards geometrical accuracy, wherein the magnitude of the total pressure difference is shown to stabilise after the application of 555,826 cells. The raw data for the mesh refinement process can be identified within Section 8.5 of the Appendix.

The mesh refinement process can be seen to involve the adjustment of the minimum and maximum levels of cell refinement within the control file of the *snappyHexMesh* dictionary. The minimum and maximum levels of refinement define the global level and custom level of cell size refinement, where the custom level is applied given a change in angle above a threshold value. The overall results presented indicate that the minimum and maximum refinement levels required were that of 2 and 7 respectively, in order to prevent the loss of topological data. In addition, the minimum threshold angle was established to be that of 30°.

An important function within the *snappyHexMesh* tool is that of the ability to apply a refinement zone to a region of the control domain, within which a defined level of refinement

is applied to all cells within it. This works to ensure that a suitable mesh resolution is applied to specific areas of geometrical interest. The results of the mesh refinement process presented an increase in the maximum skewness of a number of cells from 4.24° to 2.60°, but an increase in the average non-orthogonality of the control domain from 12.75 to 16.329 with the application of a refinement zone surrounding that of the root structure. The maximum skewness parameter is important when assessing the overall accuracy of the results as highly skewed cells can be seen to bring about simulation instability. In comparison to the maximum skewness, the average non orthogonality parameter can be seen to assess the alignment of three dimensional cells, where excessively large magnitudes may bring about instability problems (SE Norris 2006). Thus, the effective quality of the mesh is dependent upon a low skewness level and a small average non-orthogonality. From this assessment, it was established that the application of a refinement zone would increase computational time and decrease the accuracy of the results, thus a refinement region was neglected from the model.

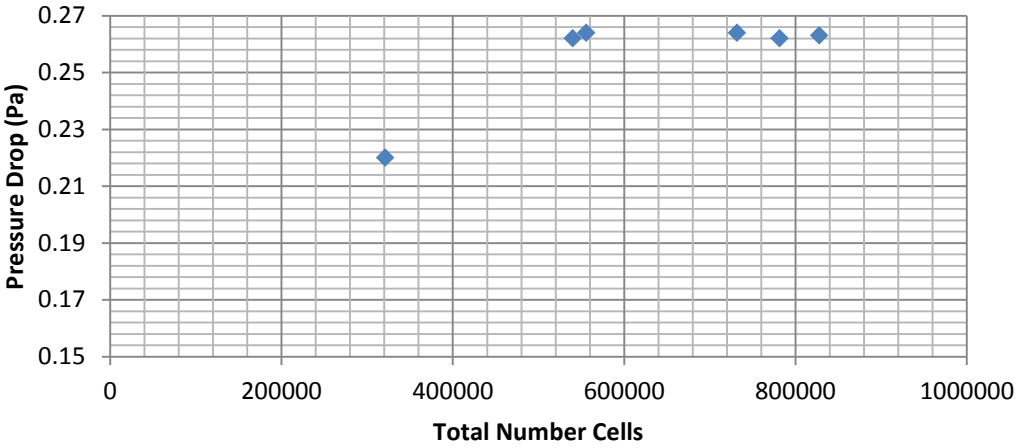

Figure 24 – Graphical representation of the convergence of the mesh towards geometrical accuracy

4.2.2 Effects of Root Architecture upon soil Hydraulic Conductivity

The results of the computational study are presented in Figure 25, wherein the pressure drop over the depth of the container has been analysed for a number of inlet velocities and contrasted to that of the pressure drop across the same porous medium region without the presence of root architecture. The results presented were established through the application of a global volumetric flux parameter to that of the root architecture boundary. This absorption parameter is based upon a derived transpiration rate of 41.7mmday^{-1}, which can be seen to correlate to a constant volumetric flow rate of 5.7x10^{-7}m^{3}s^{-1} across the surface of the model. The derived transpiration rate was acquired through the utilisation of the Penman Monteith equation, which has been tailored to that of the dimensions of the 2.2m high subject tree. Finally, a key point to note is that of the total percentage volume of roots within the control domain, V_r, where V_r=0.018%. This can be seen to be due to an extremely small branch diameter (2mm) at the root tips.

A graphical presentation of the comparative hydraulic conductivity, k, for a porous region and a porous region occupied by root structures is presented in Figure 26. The magnitude of hydraulic conductivity can be seen to be established through an assessment of the gradient of the trend, as presented by Darcy's Law (equation 3.1). The key findings from this data were such that the hydraulic conductivity differs by a magnitude of 1x10^{-5}ms^{-1} at a distance

of x=0.3m from the root structure. The derived value for the hydraulic conductivity of the porous medium containing roots structures can be seen to be dependent upon a pressure difference that is unaffected by root structures. However, the pressure drop over the porous region was also analysed at 0.05m increments in the x and y directions from the position of the main stem, as presented within Figure 30. The results of the changes in average pressure drop along sample lines *A* and *B* are presented in Figure 26, wherein the pressure drop is shown to increase towards a constant magnitude with increased distance from the vertical stem for the given inlet velocities. This is illustrated in more detail by the pressure contour plots presented in Figures 27 and 28, which contrast the fluid pressure distribution for the porous region and the porous region with roots.

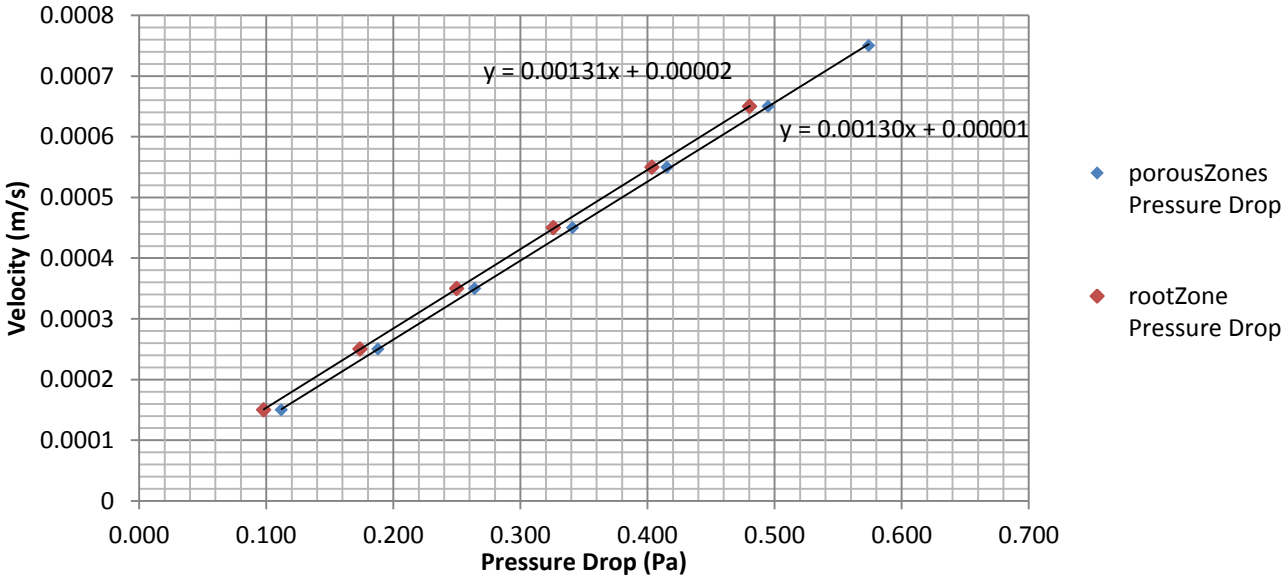

Figure 25 – Comparison of the hydraulic conductivity of a porous region not occupied by root structures to that of a region which incorporates root architecture.

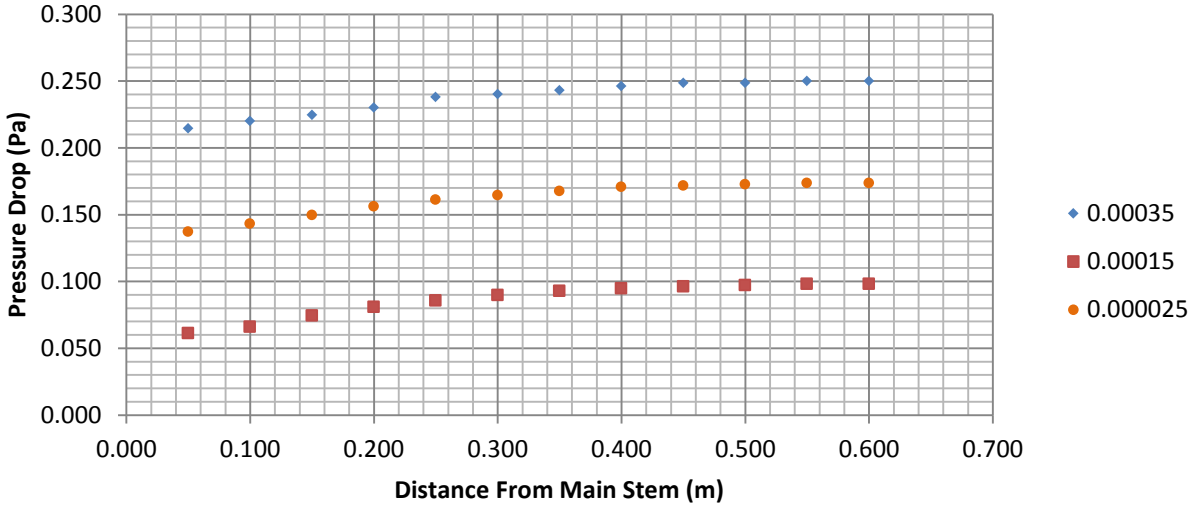

Figure 26 – Comparison of the changes in total pressure with distance from the main stem for increasing velocities

Principally, the changes in pressure difference with distance from the main stem were shown to bring about an increase in the soil hydraulic conductivity with increased distance from the stem. When examining the changes in hydraulic conductivity with distance from the stem, the magnitude of k was revealed to decrease exponentially to a constant magnitude of $k=1.3122x10^{-3}ms^{-1}$ at d=0.25m, where d is the horizontal distance from the centre of the main stem. This is illustrated within Figure 29 below, which contrasts the changes in hydraulic conductivity with distance from the root structure. A key point to note would be that of the stabilised magnitude of hydraulic conductivity for the root model, which can be seen to be equal to the hydraulic conductivity parameter for the porous zone model which is not populated by root architecture.

Figure 27 – Pressure contour plot of a porous region not occupied by root architecture

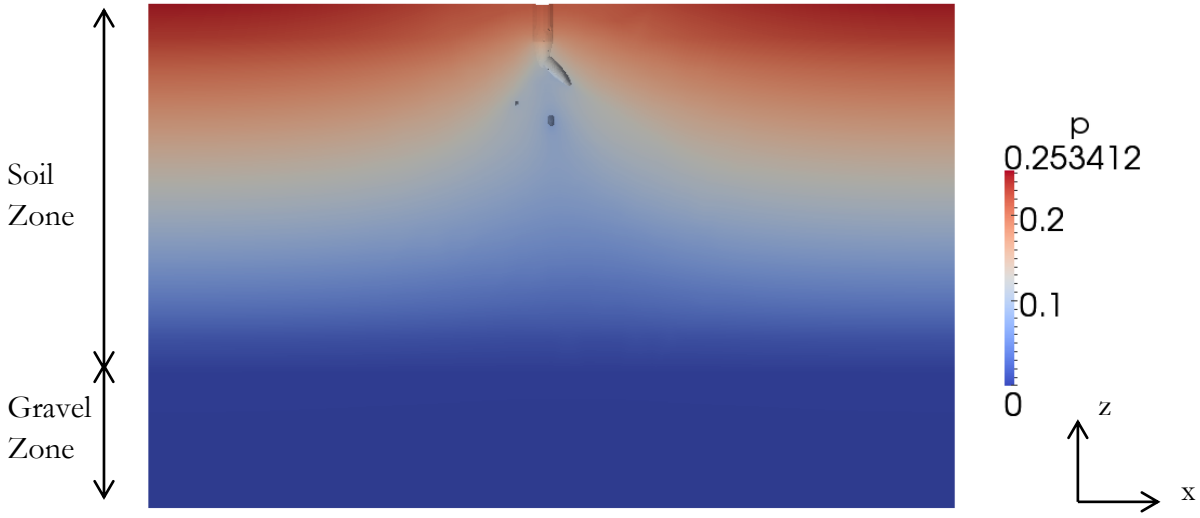

Figure 28 –Pressure contour plot of a porous region containing root architecture

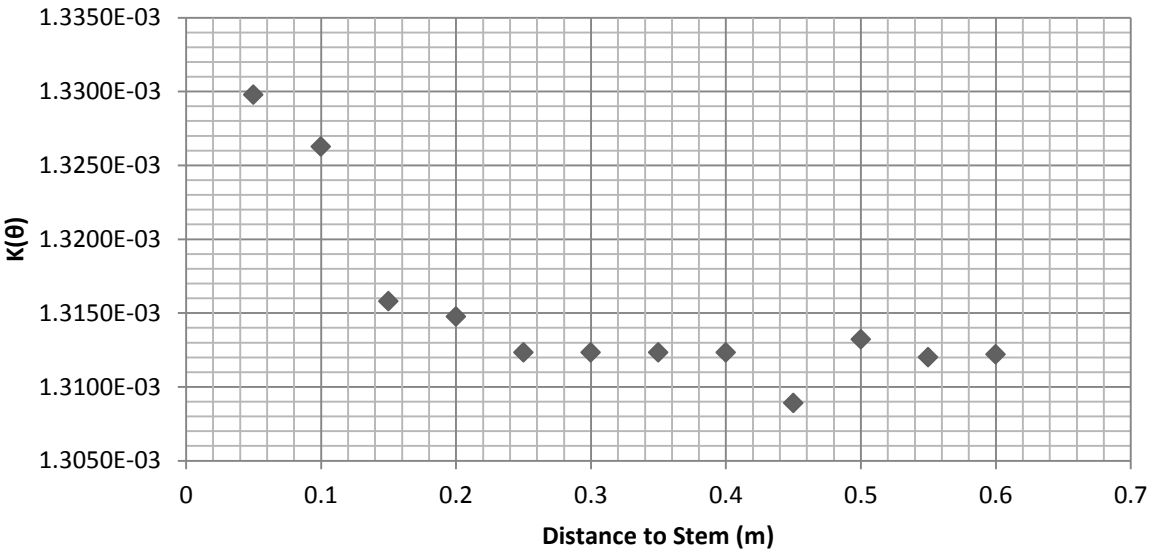

Figure 29 – Description of the changes in the hydraulic conductivity of soil with distance from the main stem

A suitable conclusion to draw from this study would be that of the effects of the root architecture upon the hydraulic conductivity of the surrounding soil, wherein the introduction of an absorption system has been shown to alter the flow pathways of the fluid moving though the porous medium. Since the hydraulic conductivity is a property of both the soil structure and that of the fluid moving through it, the introduction of a pressure driven system will inevitably bring about an increase in the magnitude of the hydraulic conductivity in the immediate area, since it works to induce changes in the nature of flow. It is important to note, however, that the variations in hydraulic conductivity of the soil are seen only within close proximity to the root model, thus suggesting that the spatial changes in magnitude are dependent upon that of the geometry of the root architecture.

In order to assess the degree to which the topology of the root structure affects the magnitude of the hydraulic conductivity, the changes in pressure difference between the inlet and outlet faces were examined in two specific directions; one which follows that of a root branch and one which moves through a region of the surrounding domain that is not populated by root structures. These directions are presented in Figure 30, where *Sample Line C* can be seen to follow a root branch of length d=0.232m and *Sample Line D* is shown to move in the negative x-direction.

The results presented in Figure 31 describe the comparative changes in the hydraulic conductivity of the surrounding soil with increased distance from the centre of the root stem for Sample Lines *C* and *D*. The key observations to note would be that of the similarities in the trend, but also the key differences in magnitude of hydraulic conductivity. Specifically, the trend of *Sample Line C* can be seen differ very little from that of the data presented in Figure 29, where the only key difference is related to the stabilisation of the hydraulic conductivity after an increased distance of 0.3m for *Sample Line C*. This suggests that the adjacent root structure has affected the hydraulic conductivity, but also that the results of the previous assessment have been somewhat validated. In contrast to this data, *Sample Line D* can be seen to present a constant magnitude of hydraulic conductivity after a distance of d=0.4m from the stem and is shown to produce a shallower gradient than that of *Sample Line C*. Thus we can establish that

the effects of root mass upon the hydraulic conductivity of the surrounding soil are not symmetrical, but are based upon the architecture of the model. In addition, we can see that the effects of the root structure upon the hydraulic conductivity extend beyond that of the end of the branch and therefore that fluid is being drawn into the system from a given distance beyond the tip. This is demonstrated by the formation of a stable hydraulic conductivity value at a distance of d=0.45m for *Sample Line D*, which can be seen to be only 0.232m long.

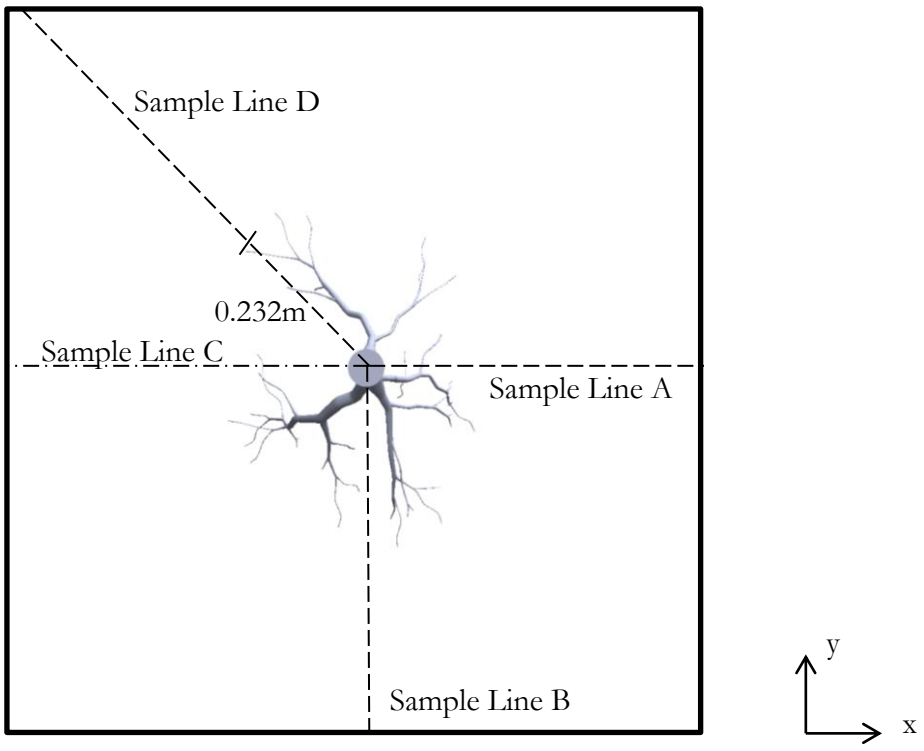

Figure 30 - Schematic presenting the positions of sample data lines

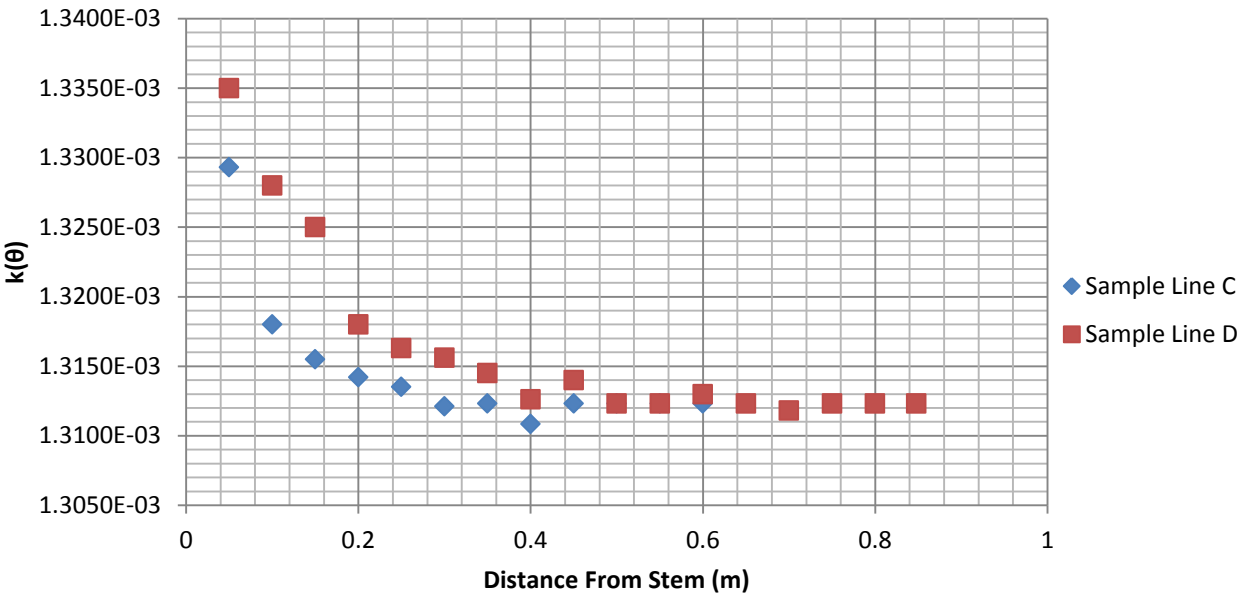

Figure 31 – Comparative changes in hydraulic conductivity along sample lines C and D

Overall, the assessment of flow around a macro-scale root system has shown that, with increased proximity to the stem, a maximum 1.3% increase in the soil hydraulic conductivity can be identified. These variations have been shown to be dependent upon the structure of the root architecture, where a greater hydraulic conductivity has been established in line with that of the root branches. These changes have also been recognised for a set distance from the branch tip. Therefore the behaviour can only be attributed to areas within close proximity to the root structures.

5.0 The *Hydro Filterra™* Model

5.2 Establishing a Representation of the *Hydro Filterra™* System

Specific aspects of the *Hydro Filterra™* bioretention system have been investigated both experimentally and computationally by other members of the group. The primary areas of the study can be seen to include that of an analysis of the soil region and an investigation of the external features of the system, such as the properties of the container and the characteristics of the inlet vents. In order to bring together the key aspects of the computational work, an attempt was made to establish a complete model of the system and to define the flow characteristics of fluid moving through the arrangement as a whole.

The specific areas of the computational study can be seen to include that of work by J. Tarrant, which assesses the nature of the flow along the surface of the adjacent road and the movement of fluid through the inlet vents; work by S. Pavey, which presents a description of the movement of fluid through the porous medium and then through the system outlet; and work by J. Ronald, which assesses the effects of root architecture upon the nature of flow through the porous region.

Using the individual models of the work above, a collaborative computational model was devised, which represents that of the *Hydro Filterra™* unit and the adjacent road surface. This model is presented in Figure 32. The model can be seen to integrate an energy dissipating stone below the inlet channels and the macro scale root architecture model previously discussed in the report. Additionally, the road surface can be seen to incorporate a 0.029° gradient, as used within work by J. Tarrant, and an outlet pipe section, which follows with that of the *Hydro Filterra™* design. (*Hydro Filterra™* System Design Plans).

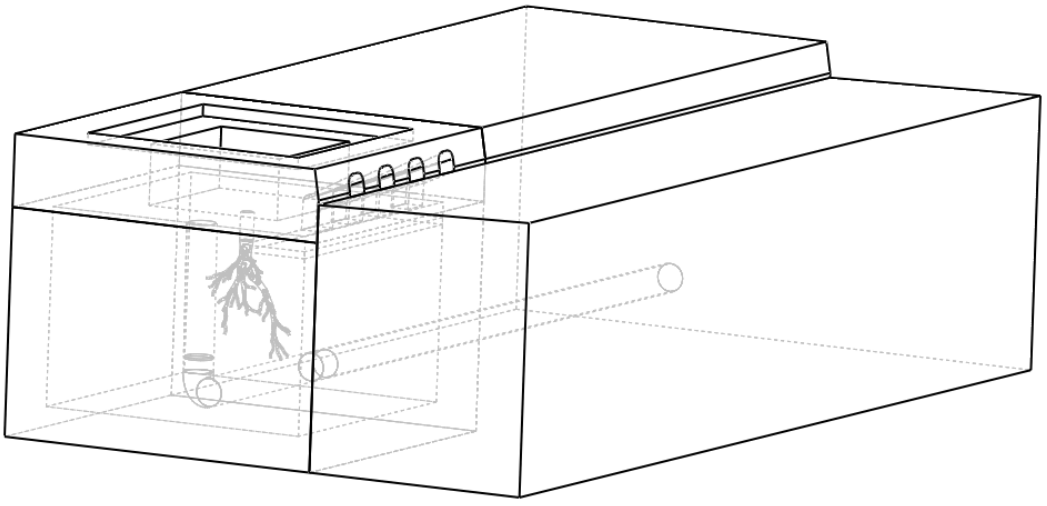

Figure 32 – Computational model of the Hydro Filterra™ bioretention system and the surrounding road surface

A computational mesh of the geometry is presented in Figure 33, which was established through the utilisation of the *snappyHexMesh* function within OpenFOAM 2.0.1. The mesh was completed in 627.5 seconds and has a maximum cell skewness of 3.14° with no highly skewed cells. The geometry presented can be seen to consist of an assembly of eight specific parts. Thus, the meshing process involved the application of a specific level of refinement to each component in order to optimise mesh quality.

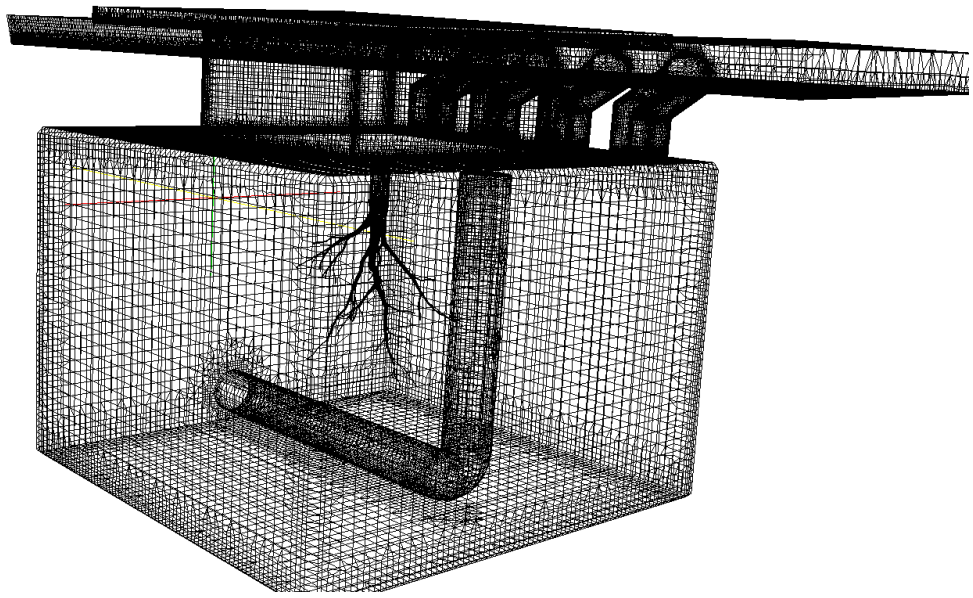

Figure 33 – Computational mesh of the case geometry

5.3 Results of the *Hydro Filterra*™ Simulation

The initial conditions of the simulation consisted of a 35mm high volume of water occupying the region in front of the unit inlet vents, with the internal volume of the unit defined as that of a body of air, as presented in Figure 34. This initial setup was aimed at representing the movement of fluid into a completely unsaturated soil region after a period of heavy rainfall, thus demonstrating a worst case scenario for the case study.

The incorporated solver was that of porousInterFoam as it was considered to be the most capable for cases involving multiphase flow through a porous medium. Additionally, porousInterFoam can be seen to utilise the Volume of Fluid (VOF) method to accurately simulate the free surface interface between two specific phases, whilst still having the capability to solve for fluid movement through a porous medium. An ideal solver would be that of a version of twoPhaseEulerFoam which has the capabilities to assess the flow of fluid through a porous region. Specifically, twoPhaseEulerFoam is a solver that is suited to a case that incorporates two incompressible fluids, where one phase is a dispersed phase. Thus, one could consider the volume of air as an immiscible fluid with a dispersed water phase moving through it. However, twoPhaseEulerFoam currently has no applications for cases that incorporate a porous medium and therefore is unsuitable for the case geometry.

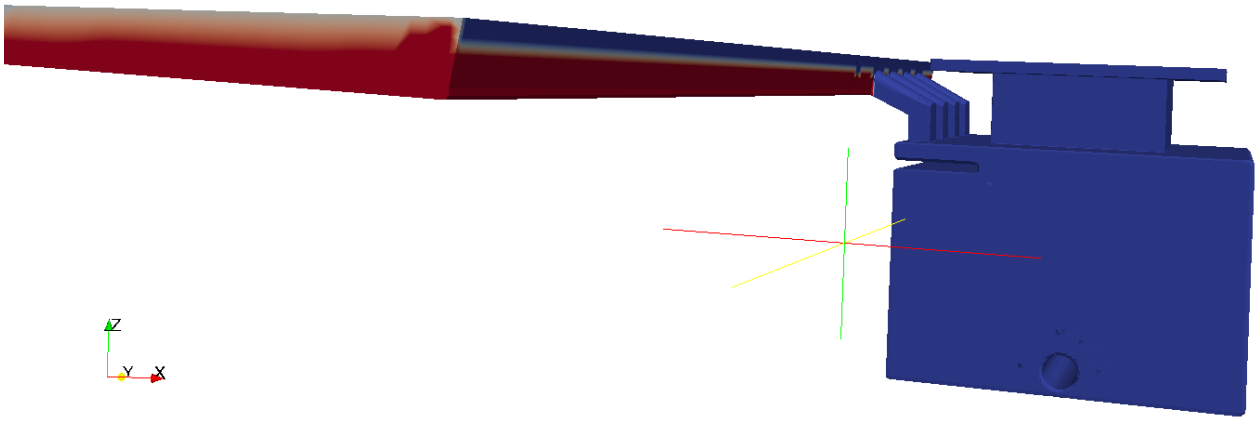

Figure 34 – Three dimensional representation of the case geometry at time step t=0

A key problem with the case presented is that of the implementation of a volume of fluid on top of a volume of air, where the only driving force is that of gravity. This setup was shown to bring about a high level of simulation instability and thus prevented the case from being fully solved. Principally, the setup was shown to bring about a case of Rayleigh Taylor instability, wherein instability is brought about at the interface between two phases of different density. This can be seen to be specific to cases where gravity is acting upon a dense fluid which has been placed on top of a less dense fluid. The resulting effect is that of unstable disturbances at the interface when the less dense fluid is displaced upwards, given the effective vertical movement of the denser fluid under gravity (Lord Rayleigh and G.I. Taylor). This effect has been studied in detail by work by S. Pavey, which investigates the principal methodology for simulating multiphase flow through a porous soil region.

6.0 Conclusions

The micro-scale findings present increases in the radial conductivity of root structures with increased root diameter. The values derived from CT scan techniques were shown to present a good fit with that of external experimental work and to theoretical models. The key limitations to the mathematical model have been highlighted by the incorporation of root tip geometry, wherein an underestimation of the theoretical magnitude is brought about by a lower flow velocity across the root boundary. A visual assessment of the total fluid pressure within the surrounding region revealed changes in soil hydraulic conductivity with distance from the root topology and a valid assessment of the impacts of root proximity indicated disproportional flow into that of the structure with the greatest radius.

A macro-scale assessment of a porous region containing root architecture revealed a maximum increase in hydraulic conductivity of 1.3% with increased distance toward the root system. This was subsequently identified to be dependent upon the structure of the root architecture, where an increase in hydraulic conductivity was presented following that of a root branch. Moreover, the study presents a reduction in the effects of root branch topology given a set distance from the branch tip. The hydraulic conductivity at these positions was recognised to match that of a porous medium which was not occupied by root structures.

The key aims of the project have been met through the analysis of root systems on two scales. A macro-scale assessment of flow around a plant root network has allowed for the

evaluation of root topology upon the flow characteristics of a porous medium. Additionally, the investigation of the flow pathways of a porous medium populated by root structures has been achieved on the micro-scale. However, the results have not been contrasted to completed experimental work and therefore are only validated by external sources. In addition the assumptions of the models, such as that of the generalisation of the root architecture and the disregard for soil particle compaction, are possible causes for error within the macro-scale and micro-scale models respectively.

Finally, the completion of work by additional members of the project group has allowed for the availability of information within. The level of work undertaken by each individual has mostly followed with that of the scheduled deadlines and thus the majority of work has been unhindered. On an individual basis, the completion of work has been largely interrupted by problems regarding the computational discretisation of the micro-scale system. This meant that several of the proposed deadlines were to be extended, as presented within the gantt chart below, which illustrates the individual targets and group deadlines. Nevertheless, the key aims of the project have been met within the given time frame and a suitable degree of accuracy has been incorporated into the results.

A suitable advancement of this work would be to assess the effects of root tip geometry upon the radial absorption parameter using the micro-CT techniques presented. Alternatively, the effects of soil compaction could be investigated for root structures of differing topology. These aspects have been shown to be critical in establishing an accurate magnitude of radial conductivity and thus require further investigation. A final continuation of the study may include that of analysing the impacts of soil saturation upon the magnitude of root conductivity, thus allowing for the establishment of a more accurate computational model.

Acknowledgements

Lesley Wears for her contributions regarding the acquisition of micro CT data and her cooperation during a busy period.

Daniel Jarman and Mark Goodger for their contributions to the project and their assistance during a field trip to Barry, Wales.

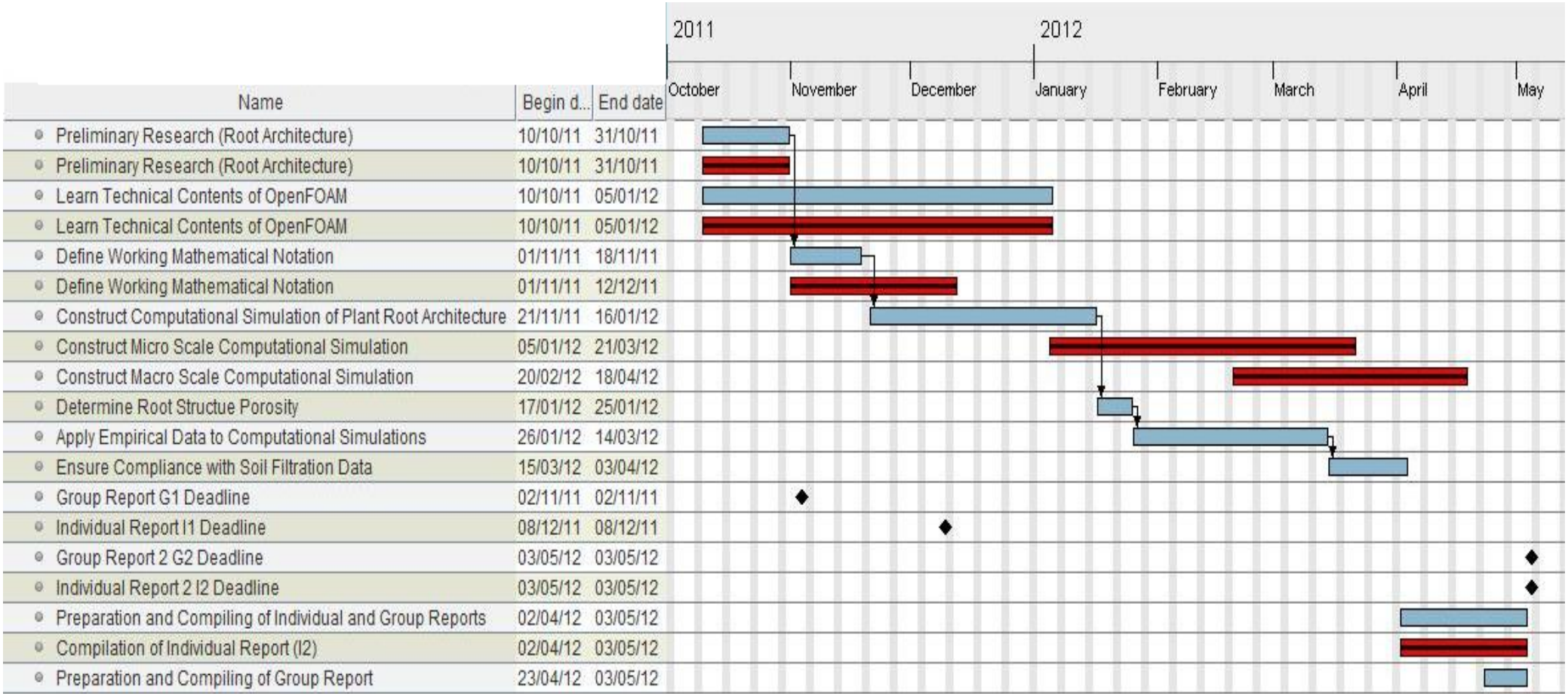

Name	Begin d...	End date
Preliminary Research (Root Architecture)	10/10/11	31/10/11
Preliminary Research (Root Architecture)	10/10/11	31/10/11
Learn Technical Contents of OpenFOAM	10/10/11	05/01/12
Learn Technical Contents of OpenFOAM	10/10/11	05/01/12
Define Working Mathematical Notation	01/11/11	18/11/11
Define Working Mathematical Notation	01/11/11	12/12/11
Construct Computational Simulation of Plant Root Architecture	21/11/11	16/01/12
Construct Micro Scale Computational Simulation	05/01/12	21/03/12
Construct Macro Scale Computational Simulation	20/02/12	18/04/12
Determine Root Structue Porosity	17/01/12	25/01/12
Apply Empirical Data to Computational Simulations	26/01/12	14/03/12
Ensure Compliance with Soil Filtration Data	15/03/12	03/04/12
Group Report G1 Deadline	02/11/11	02/11/11
Individual Report I1 Deadline	08/12/11	08/12/11
Group Report 2 G2 Deadline	03/05/12	03/05/12
Individual Report 2 I2 Deadline	03/05/12	03/05/12
Preparation and Compiling of Individual and Group Reports	02/04/12	03/05/12
Compilation of Individual Report (I2)	02/04/12	03/05/12
Preparation and Compiling of Group Report	23/04/12	03/05/12

Key

Scheduled Tasks

Completed Tasks

7.0 References

Akgiray, O. and Saatçı, A. M. "Water Science and Technology" Water Supply, Vol:1, Issue:2, pp.65-72, 2001.

Abeysekera, R.M., McCully, M.E., (1993) "Development in Normal Roots" *Department of Biology, Carlton University, Ottawa,* 413-429

Angers, D.A., and Caron, J., (1998)" Plant-Induced Changes in Soil Structure: Processes and Feedbacks" Bio-geochemistry, 2nd Edition

Begley, A., Pavey, S., Please, J., Ronald, J., Russell, S., Tarrant, J., Whitehurst, L., Winston-Gore, S., (2011) "*Investigating Storm Water Filters And Bioretention Systems*", 1-10

Begley, A., (2012) "Three Dimensional Image Based Meshing and Computational Analysis of Fluid Flow in Various Porous Media" *Investigation of Stormwater Filters and Bioretention Systems*

Brown, T.N., Kulasiri, D., Gaunt, R.E., (1996), "A Root Morphology Based Simulation For Plant/Soil Microbial Ecosystem Modelling", (99) 275-287

Chatterjee, P.K., Gupta, B.S., Absorbent Technology – Textile Science and Technology, First Edition 2002

Clark, S., Pitt, R., (2009), "Metals Removal Technologies for Stormwater" *Proceedings of the Water Environment Federation*, 739-765(25)

Erpenbeck J. M. (1981) "A Methodology to Estimate Marram Grass Water Requirements in a Dune Environment" *Washington State University,* 233-247

Feddes, R.A., Kowalik, P., Zaradny, H., (1974) "Simulation of Field Water Uptake By Plants Using A Soil Water Dependent Root Extraction Function", *Journal of Hydrology*, (31) 13-26.

Feddes, R.A., Raats, P.A.C., (2004). "Parameterizing The Soil-Water Plant Root System", *Modelling: Progress, Challenges and Applications,* 245-251

Hector, D.J., Gregson, K., McGowan., (1992), "A Computer Simulation Describing Water Extraction By Crop Root Systems", (32) 287-304

Hooker, H. D., (1986) "Hydrotropism in Roots of Lupinus Albus" (24) 265-283

Horn, R., Taubner, H., Wuttke, M., Baumgartl, T., (1994) "Soil Physics Properties Related To Soil Structure" (30) 187-216

Howell, T.A., J.L. Steiner, A.D. Schneider, S.R. Evett, and J.A. Tolk. (1997) "Seasonal And Maximum Daily Evapotranspiration Of Irrigated Winter Wheat" 40(3) 623-634.

Hydro International (UK) – *Hydro Filterra*: Advanced Bioretention System for Stormwater Treatment: Design Guide
http://www.hydro-international.biz/media/Filterra%20Design%20Manual%20A0611.pdf

Hydro International (UK) – *Hydro Filterra*: Plant Selection Guide for Stormwater Bioretention Systems

Lontoc Roy, M., Dutilleul, P., Prashar, O.S., (2006) "Advances in the acquisition and analysis of CT scan data to isolate a crop root system from the soil medium and quantify root system complexity in 3-D space", 231-241

Looomis R. S., W. A. Williams (1969) "Productivity and the Morphology of Crop Strands" *Physiological Aspects of Crop Yield*, 27-47

Lord R. Taylor, J. W. Strutt (1883) "Investigation of the character of the equilibrium of an incompressible heavy fluid of variable density". *Proceedings of the London Mathematical Society* (14) 170-177

Monteith J.L (1981) "Evaporation and Surface Temperature" Meteorological Society (107) 1-27

Monteith, J.L. (1965) "Evaporation and environment modelling" (19) 205-224

Molisch, H., Sachs, J.F., (1983), "Properties of Hydrotropism" 857-913

Nemirovsky, J., lifshitz, A., Be'erya, I., (2011), "Tomographic Reconstruction Of Incompressible Flow" (82) 1-5

Neumann, G., Romheld, V., (2002) Root-Induced Changes in The Availability Of Nutrients In The Rhizosphere" (36) 617‑649

Pavey, S. (2012) "Macro Scale Computational Analysis Including Porous Media and Free Surface Interaction" *Investigation of Stormwater Filters and Bioretention Systems*

Please, J., (2012) "Micro Scale Experimental Investigation to Determine the Pore Geometries of the Hydro Filterra Bioretention Media with Experimental Validation to Computational Models Using Additive Layer Manufacturing Techniques" *Investigation of Stormwater Filters and Bioretention Systems*

Richards, L.A., (1931), "Capillary Conduction Of Fluid Through Porous Mediums", *Physics* 1, 318‑3343.

Sharma M. L. (1985) "Estimating Evapotranspiration" *Advances in Irrigation* p213-281

S.E. Norris 2006 "Finite Volume Methods for Non-Orthogonal Meshes"

http://ses.library.usyd.edu.au/bitstream/2123/376/4/adt-U20010730.12021506_chapter_5.pdf

Simunek, J, Hopmans, J.W., (2004) "Modelling Compensated Root Water Uptake" *Department of Environmental Sciences, University of California Riverside, (*220*)* 505-521

Tarrant, J., (2012) "Macro Scale Computational Analysis of the *Hydro Filterra* Stormwater Drainage System in an Industrial Urban Environment" *Investigation of Stormwater Filters and Bioretention Systems*

Van Genuchten, M. T (1980) "A Closed–Form Equation for Predicting The Hydraulic Conductivity Of Unsaturated Soils", *journal of Soil Science*, (44**)**, 892–898.

Vercambre, G., C. Doussan, L. Pages, R. Habib, A. Pierret., (2002), "Influence of xylem development on axial hydraulic conductance within Prunis root systems". Volume: 16, Issue: 7, Pages: 479-487

Washburn, W. E. (1921). "The Dynamics of Capillary Flow"

Whitehurst, L., (2012) "Macro Scale Experimental Investigation to Determine the Hydraulic Properties of the Hydro Filterra Bioretention System with Comparison to the Hydraulic Performance of the Case Study" *Investigation of Stormwater Filters and Bioretention Systems*

Wilderotter, O., (2001), "Adaptive Finite-Elemente Methoden for Singular Parabolic Problem", 452-523

8.0 Appendix

8.1 The Van Genuchten Model

The relationship between soil water content, θ, and soil water pressure head, h, is presented through the utilisation of a water retention curve, characteristic to different types of soil. When plotted against each other, decreases in soil water content are shown to generate increases in pressure head due to raised soil surface tension and capillary forces at lower levels of soil saturation (Van Genuchten 1980). The graph suitably describes the relationship between the two parameters, but requires an experimental assessment of soil moisture potential, which must be obtained using tensiometer testing. The profile of the water retention curve can, however, be characterised through the use of the Van Genuchten approach (Van Genuchten 1980), which incorporates four key parameters to define the shape of the curve:

$$\theta(h) = \theta r + \frac{\theta s - \theta r}{[1+(\alpha h)^n]^{1-1/n}} \qquad (8.1)$$

Here, θr [m^3m^{-3}] and θs [m^3m^{-3}] represent the residual and saturated soil water content respectively and θ(h) represents the function for changes in soil water content with pressure head, as depicted by the water retention curve. The parameters α [m^{-1}] and n relate to the inverse of air suction and the pore size distribution respectively. The parameters α>0 and n>1 must be defined experimentally for specific soils and the residual and saturated soil water contents must be established soil saturation testing.

8.2 Penman Monteith Equation

The Penman Monteith Equation is an estimation of the daily water consumption budget of a given plant species. It is commonly used within irrigation system design and crop yield simulations and is therefore an important method to consider. The Penman Montieth equation presented in equation (3.4) can be seen to incorporate a number of parameters such as that of the aerodynamics resistance of the plant, R_c [sm^{-1}]:

$$R_a = \frac{\left[\ln\left(\frac{z_m - d}{z_{om}}\right)\right]\left[\ln\left(\frac{z_h - d}{z_{oh}}\right)\right]}{k^2 u_z} \qquad (8.2)$$

Where z_m [m] is the height of the wind measurement, z_h [m] is the height of the air and humidity measurements with respect to the ground surface, d [m] is the zero plane displacement height of the measurement surface, z_{om} [m] is the roughness length for momentum transfer, z_{oh} [m] is the roughness length for the momentum transfer, k is the von Karman constant for turbulent diffusion (k=0.41) and u_z [ms^{-1}] is the wind speed at height z. Typically:

$$z_{om} = 0.0123 h_c \qquad (8.3)$$

$$z_{oh} = 0.0123 h_c \qquad (8.4)$$

$$d = 0.067 h_c \qquad (8.5)$$

Where h_c [m] is the mean height of vegetation
and

$$r_c = \frac{r_1}{0.5\ LAI} \qquad (8.6)$$

Where r_1 [sm^{-1}] is the average daytime value of stomatal resistance for a single leaf, which is approximated as $100sm^{-1}$ for tree canopies with height exceeding 4m (Monteith 1981 and Sharma 1985). The parameter LAI is the Leaf Area Index and r_c [sm^{-1}] is the bulk stomatal resistance.

Work undertaken by Loomis and Williams (Loomis and Williams 1969) has shown that the leaf area index has been shown to be approximated to:

$$LAI = 5.5 + 1.5\ln(h_c) \qquad (8.7)$$

The average daily soil heat flux, G, was approximated according to work by (Wright and Jenson) as:

$$G = (T_a - T_p)\ C_s \qquad (8.8)$$

Where T_a and T_p [°C] are the average daily air temperature and the average daily air temperature from the previous day, respectively, and C_s [MJ m^{-2} d^{-1} °C^{-1}].

The parameter Δ [K^{-1} kg m^{-1} s^{-2}] can be defined as the rate of change of saturation specific humidity with air temperature and can be defined through the utilisation of equation 8.9, which has been used within work by Erpenback (1981) to assess the changes in fluid consumption of Marram grass with humidity:

$$\Delta = \frac{4098\ e^0}{(T+237.3)^2} \qquad (8.9)$$

$$e^0 = exp\left[\frac{16.78T-117}{T+237.3}\right] \qquad (8.10)$$

Where e^0[kPa] is the saturation vapour pressure at temperature, T[°C], which is taken as T_a.

Finally, the psychometric constant, γ [kPa °C^{-1}] was calculated as:

$$\gamma = \frac{C_p P}{\varepsilon\ \lambda} \qquad (8.11)$$

Where λ [MJ kg-1] is the latent heat of vaporisation, which is based upon T_a, and ε is the ratio of the molecular weights of air to water (~0.622)

The atmospheric pressure, P [kPa], was taken as P=101kPa; the specific heat capacity of air at constant pressure, c_p [MJ kg^{-1} $°C^{-1}$], was established as c_p=33.3, which is based upon the heat capacity ratio.

8.3 Penman Monteith Variables

Climate Based	Magnitude	Variable	Magnitude	Variable	Magnitude	Variable	Magnitude
Ta	17	**rn**	1.11E+02	**G**	-2.63158	rc	42.2497
Tp	18	zm	2	ta	17	LAI	4.734
Uz	0.89	zh	2	tp	18	**r1**	100
	1.5	d	0.402	cs	0.38		
rn	1.11E+02	zom	0.0738				
ga	0.0257	zoh	0.00738				
z	1.5	k	0.41				
rc	42.2497					**Variable**	**Magnitude**
cp	33.50794					**y**	1.33
y	1.33					P	101
G	-2.63158					ep, e	0.622
Δ	0.122842					lambda	2.456
Ea-ed	0.001199					cp	33.508

Figure 35 – Table of values containing the parameters presented in equations (8.0) to (8.11)

8.4 Micro-Scale Investigation Data

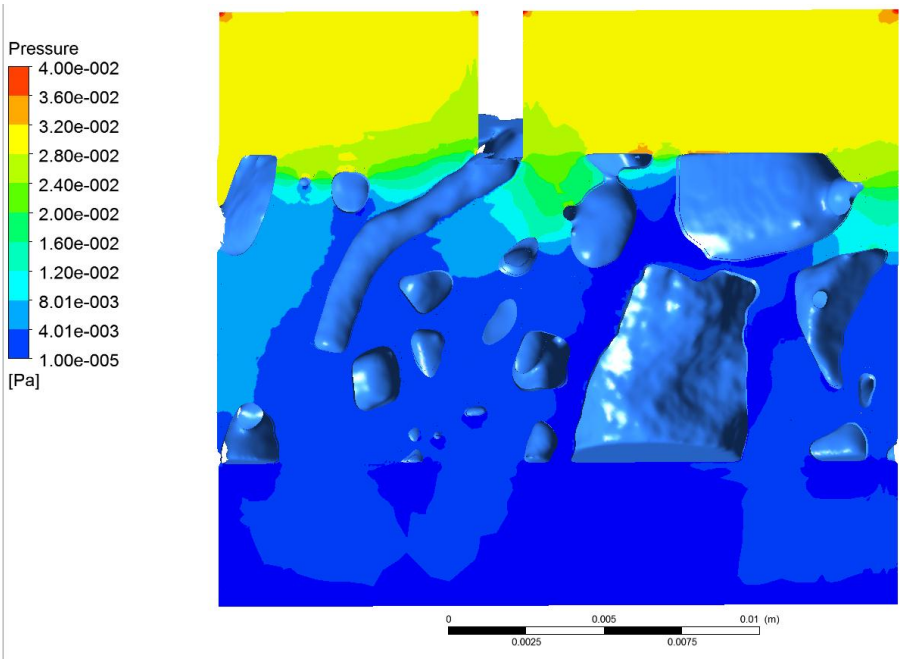

Figure 36 – Pressure contour plot for the slice Plane 2

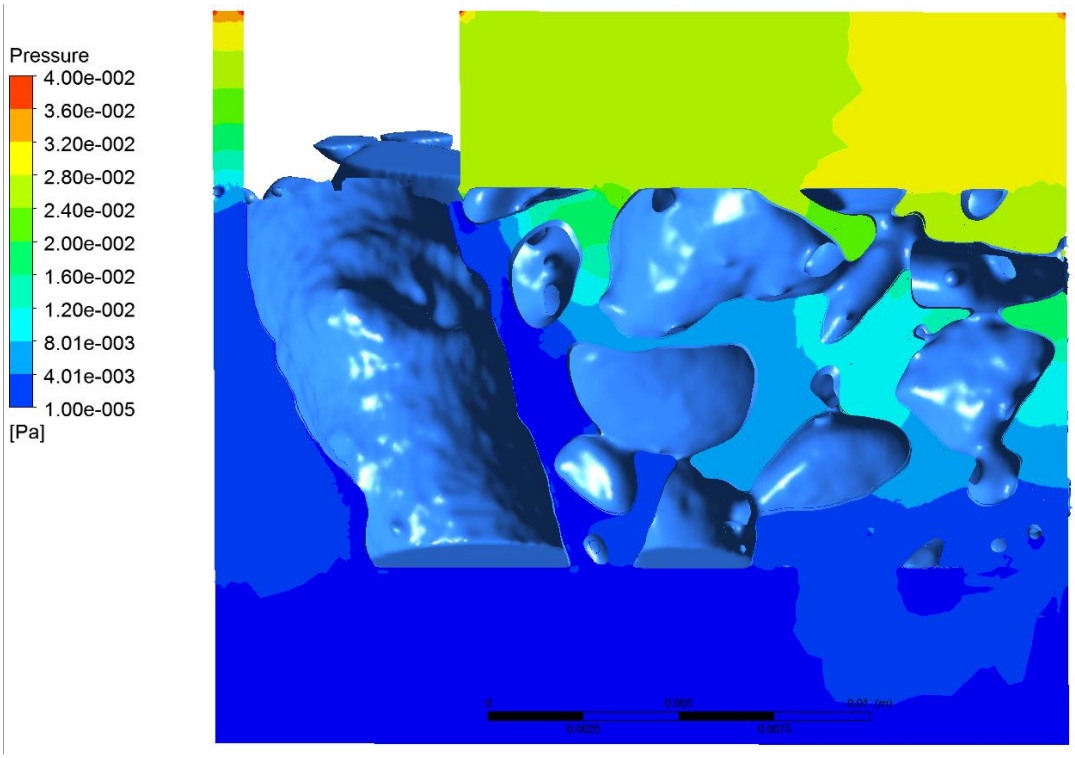

Figure 37 – Total Pressure contour plot for the data slice Plane 1

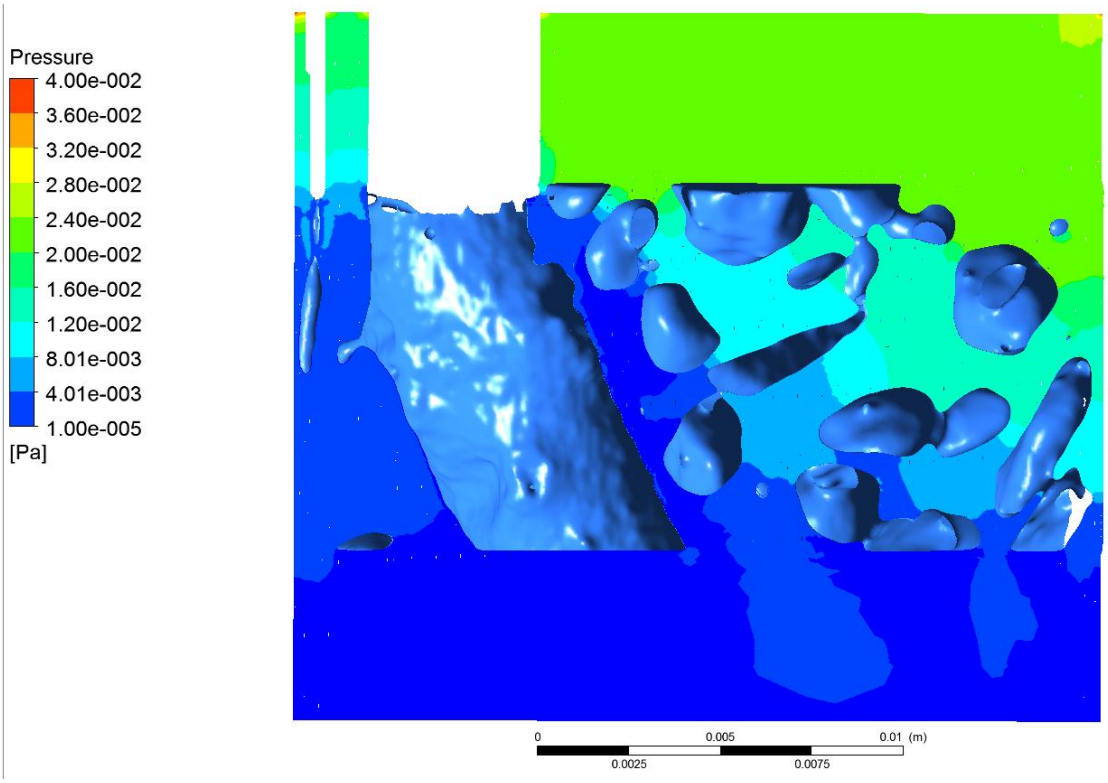

Figure 38 – Total Pressure contour plot for the data slice Plane 3

8.5 Macro Scale Investigation Data

Refinement Level	Minimum Angle (°)	No. Cells	Pressure Drop (Pa)	Max Skew (°)	Max Non Orthogonality	Average Non-Orthogonality	Refinement (Y/N)
(2 5)	50	321038	0.22	2.010	62.310	18.310	n
(2 7)	30	555826	0.264	2.599	59.294	16.673	n
(2 7)	30	828080	0.263	4.242	60.148	12.753	y
(3 7)	30	540314	0.262	4.010	61.157	16.396	n
(2 7)	30	731913	0.264	4.1853	64.610	11.292	y
(2 7)	30	781493	0.262	4.185	64.610	11.852	y

Figure 39 – Data illustrating the mesh refinement process